Article

Not peer-reviewed version

Design and Synthesis of Arylboronic Acid Chemosensors for the Fluorescent-Thin Layer Chromatography (f-TLC) Detection of Mycolactone

Gideon Atinga Akolgo , Benjamin M. Partridge , Timothy D. Craggs , Kingsley Bampoe Asiedu , Richard Kwamla Amewu *

Posted Date: 4 March 2025

doi: 10.20944/preprints202503.0093.v1

Keywords: mycolactone; Buruli ulcer; boronic acid; chemosensor; diagnosis; molecular recognition; mycolactone; *Mycobacterium ulcerans*

Article

Design and Synthesis of Arylboronic Acid Chemosensors for the Fluorescent-Thin Layer Chromatography (f-TLC) Detection of Mycolactone

Gideon Atinga Akolgo [1], Benjamin M. Partridge [2], Timothy D. Craggs [2], Kingsley Bampoe Asiedu [3] and Richard Kwamla Amewu [1,*]

[1] Department of Chemistry, University of Ghana, Legon-Accra P.O. Box LG56, Ghana

[2] School of Physical and Mathematical Sciences, Dainton Building, University of Sheffield, Sheffield, S3 7HF, UK

[3] Department of Neglected Tropical Diseases, World Health Organization, 1211 Geneva, Switzerland

* Correspondence: ramewu@ug.edu.gh

Abstract: Fluorescent chemosensors are increasingly becoming relevant in recognition chemistry due to their sensitivity, selectivity, fast response time, real-time detection capability, and low cost. Boronic acids have been reported for the recognition of mycolactone, the cytotoxin responsible for tissue damage in Buruli ulcer disease. A library of fluorescent arylboronic acid chemosensors with various signaling moieties with certain beneficial photophysical characteristics (i.e. aminoacridine, aminoquinoline, azo, BODIPY, coumarin, fluorescein, and rhodamine variants); and a recognition moiety (i.e. boronic acid unit) were rationally designed and synthesized using combinatorial approaches; purified and fully characterized using a set of complementary spectrometric and spectroscopic techniques such as NMR, LC-MS, FT-IR, and X-ray crystallography. In addition, a complete set of basic photophysical quantities such as absorption maxima (λ_{abs}^{max}), emission maxima (λ_{em}^{max}), Stokes shift ($\Delta\lambda$), molar extinction coefficient (ε), fluorescence quantum yield (Φ_F), and brightness were determined using UV-vis absorption and fluorescence emission spectroscopy techniques. The synthesized arylboronic acid chemosensors were investigated as chemosensors for mycolactone detection using the fluorescent-thin layer chromatography (f-TLC) method. Compound 7 (with a coumarin core) emerged the best (λ_{abs}^{max} = 456 nm, (λ_{em}^{max} = 590 nm, $\Delta\lambda$ = 134 nm, ε = 52816 $M^{-1}cm^{-1}$, Φ_F = 0.78, and brightness = 41197 $M^{-1}cm^{-1}$).

Keywords: mycolactone; Buruli ulcer; boronic acid; chemosensor; diagnosis; molecular recognition; mycolactone; *Mycobacterium ulcerans*

1. Introduction

Over the years, researchers, inspired by certain biological processes in nature looked for new concepts that allow for the selective molecular recognition of target molecules that play important roles in complex chemical processes in various disciplines such as medicine, biology, agriculture, biomedical, environmental, and social sciences [1]. Molecular recognition is achieved by the utility of chemosensors. Chemosensors are molecules of abiotic origin that signal the presence of matter or energy. A fluorescent chemosensor therefore is a compound that interacts with an analyte in such a way as to produce a detectable fluorescent signal [2]. Fluorescent chemosensors have been of particular interest in supramolecular chemistry because of their ability to recognise guest species as well as their high selectivity, sensitivity, and simplicity [3,4]. Generally, a fluorescent chemosensor is composed of a recognition moiety that interacts with an analyte of interest and relays the recognition event through a signalling unit. Thus, the engineering of an appropriate fluorescent chemosensor with the right recognition and signalling moieties can result in favourable interactions with specific analytes.

 doi:10.20944/preprints202503.0093.v1

A boronic acid motif can be explored as a recognition unit in the design of chemosensors to exploit the 1,3-diol moieties on the structure of the analyte. This is because boronic acids and their derivatives have been known for decades to form five- or six-membered cyclic boronate esters with both *cis*-1,2- and 1,3-diols that are present on biologically relevant molecules through covalent bonding [5–10]. The phenomenon of the complexation of boronic acids with polyols dates to over 70 years but remains an area of interest. The first reported use of boronic acids as recognition units for *cis* 1,2- or 1,3-diol-containing compounds was published by Lorand and Edwards in 1959 [11]. They demonstrated the complexation equilibria of aqueous benzeneboronate ion with several polyols and compared the association constants to that of borate. Following the early seminal work of Lorand and Edwards, boronic acids have greatly evolved into an area of research for molecular recognition thus gaining significant interest in the design of many fluorescent chemosensors. This is because of their selective binding behaviour for a considerable number of biological molecules possessing polyhydroxy motifs, their high stability, environmental friendliness, general low toxicity, and their relatively inexpensive nature. The first fluorescent boronic acid-based sensor was developed later in 1992 by Yoon and Czarnik for saccharide sensing [12]. Since then, boronic acids have attracted considerable interest in molecular recognition in which the boronic acid functionality has increasingly become a very important recognition moiety in the design and synthesis of molecular recognition chemosensors taking advantage of this unique intrinsic affinity for 1,2-cis and/or 1,3-cis diols. The selective binding behaviour of the boronic acid unit has been explored for the detection of diol-containing analytes based on the "lock-and-key" concept of enzyme-substrate recognition [1]. The unique properties of the boronic acid functionality has positioned it as an invaluable receptorhave shown great promise for the specific recognition and detection of various species in real-world situations [13]. They have become popular as sensors *for* various biological polyol molecules including *monosaccharides and in particular glucose [14]*, catecholamines [15], and dopamine. *Others include* various polysaccharides, glycoproteins and glycated haemoglobin [16–22], ionic compounds [23–25], anions such as cyanides and fluoride [9,26–28], water traces in solvents [29,30], and hydrogen peroxide (H_2O_2) [31,32]. Furthermore, boronic acids have also been employed as biochemical tools for a variety of applications, including but not limited to enzyme inhibitors [33], cell delivery methods [34], whole-body diagnostic imaging [35], and tumour cell imaging [36,37].

The pathogenesis of *Mycobacterium ulcerans* disease is widely dependent on the activity of a unique toxin called mycolactone [38]. Mycolactone plays a significant role in the virulence, pathogenicity, and cytotoxicity of Buruli ulcer (BU) disease. It has immunosuppressive properties and is responsible for the tissue damage seen in BU [39,40]. Structurally, mycolactone A/B is a polyketide macrolide toxin composed of a 12-membered macrocyclic lactone core (C1–C11) with two laterally attached side chains; a C-linked northern side chain (C12–C20) with two hydroxyl groups in 1,3-diol positions at C17 and C19; and an esterified C5-O-linked highly polyunsaturated acyl southern side chain (C1'–C16') possessing a conjugated pentaenoic acid ester chromophore and three hydroxyl groups, two of which are in 1,3-diol positions at C13' and C15' [41,42] (Figure 1).

The secretion of mycolactone is a distinguishing feature of *M. ulcerans* amongst other human mycobacteria. Hong *et al.* have established that mycolactone A/B appears to be biosynthetically restricted to *M. ulcerans*, homogeneously distributed within the infected tissue, and shown to diffuse beyond the foci of primary infection hence specific recognition of mycolactone thus key for the diagnosis of BU [43]. Histopathological studies have shown that in tissues, mycolactone is widely distributed compared to the causative organism [44]. Consequently, the detection of its presence in biological samples is necessary for the diagnosis of the disease. Based on these findings, Kishi and colleagues developed a sensitive and practical flourescent-thin layer chromatographine (f-TLC) technique for detecting the toxin. The diagnostic method utilizes the derivatization of diol motifs of mycolactone A/B using a 2-naphthylboronic acid forms six-membered cyclic boronate esters which can be detected on a TLC plate as an adduct (Figure 2). Accordingly, the 2-naphthylboronic acid and mycolactone work as an acceptor–donor FRET pair. The boronic acid unit reacts selectively with 1,3-diol(s) moieties of mycolactone to form boronate esters, significantly enhancing fluorescent intensity.

 doi:10.20944/preprints202503.0093.v1

The proposed general mechanism involves the FRET process, where a donor, in this case, the pentaenoate chromophore of mycolactone is excited at a defined wavelength (365 nm), and the energy is transferred, *via* non-radiative dipole-dipole interactions, to a properly selected acceptor (the 2-naphthylboronic acid), which emits through radiative relaxation. The free 2-naphthylboronic acid with the lowest (n–p*) excited singlet state (S1) has the lower absorptivity and so it is weakly fluorescent. On the other hand, the hybridization of boron atom plays a secondary role in affecting fluorescence intensity. Therefore, binding with mycolactone at the right temperature results in the formation of the cyclic boronate in which the hybridization of boron atom changes from sp^2 to sp^3 has the lowest (p–p*) excited singlet state and results in a large enhancement of fluorescence emission (Figure 2).

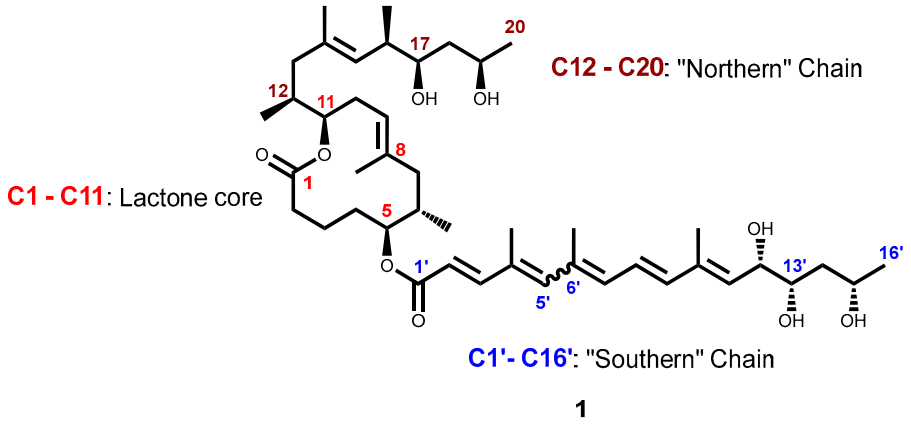

Figure 1. Structure of mycolactone A/B.

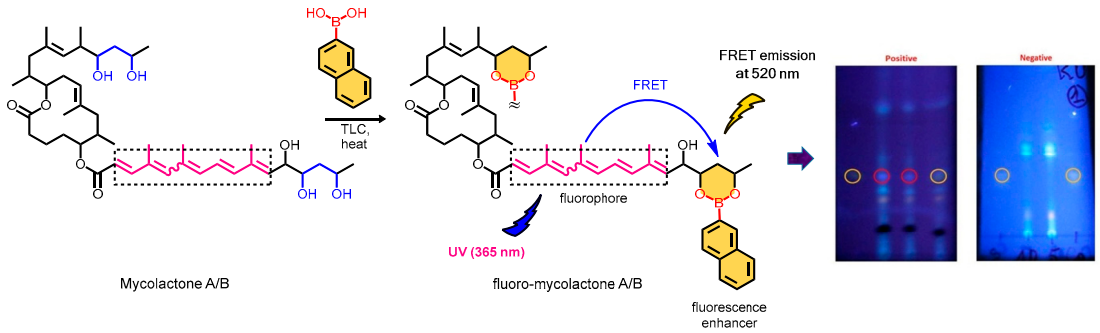

Figure 2. A schematic representation of the proposed mechanism of fluorescence of mycolactone and 2-naphthylboronic acid as observed on TLC.

Based on this principle, other commercially available boronic acids were investigated and 9,9-Diphenyl-9H-fluoren-4-yl)boronic acid (BA18) was found to be a potential alternative to 2-naphthylboronic acid (BA) [45]. The f-TLC method holds great promise because it is relatively cheap, simple to use, and rapid. [46–48]. Although the method has been successfully evaluated using clinical samples [49,50], it is hampered by the fact that it is non-quantitative. There are also concerns about interferences from other co-extracted and co-eluted lipids which make reading the results of the method subjective [49]. There is a need to improve upon the low detection and quantification rates as well as discriminate the mycolactone from other autofluorescent co-extracted human tissues. This study aimed to address these principal challenges associated with the f-TLC technique for the diagnosis of Buruli ulcer. To the best of our knowledge, no chemosensor has been designed for the molecular recognition of mycolactone. Considering the broad application of boron-based fluorescence sensors, our goal was to incorporate the boronic acid motif into various fluorescent dyes as chemosensors for mycolactone detection. Considering the unique structure of mycolactone, we hypothesised that boronate ester formation between the diol moieties of mycolactone and a boronic

Preprints.org (www.preprints.org) | NOT PEER-REVIEWED | Posted: 4 March 2025 doi:10.20944/preprints202503.0093.v1

acid binding site attached to a fluorescent molecule would allow for signal transduction that could be exploited for mycolactone detection. Therefore, we employed various fluorescent dyes (fluorophores) such as 9-aminoacridine, 8-aminoquinoline, azo, BODIPYs, coumarins, fluorescein, and rhodamines dyes, which are all amenable to boronic acid tethering to design, synthesize and characterize various fluorescent arylboronic acid dye chemosensors. These are already well-known fluorophores with excellent photophysical properties including large excitation and emission maxima, extinction coefficient, high fluorescence quantum yield (Φ), large Stokes shift, high brightness, adequate solubility, good thermal and photostability and sufficient chemical stability [51–53] (Figure 3). Secondly, these dyes are commercially available and can be coupled to diverse functional groups.

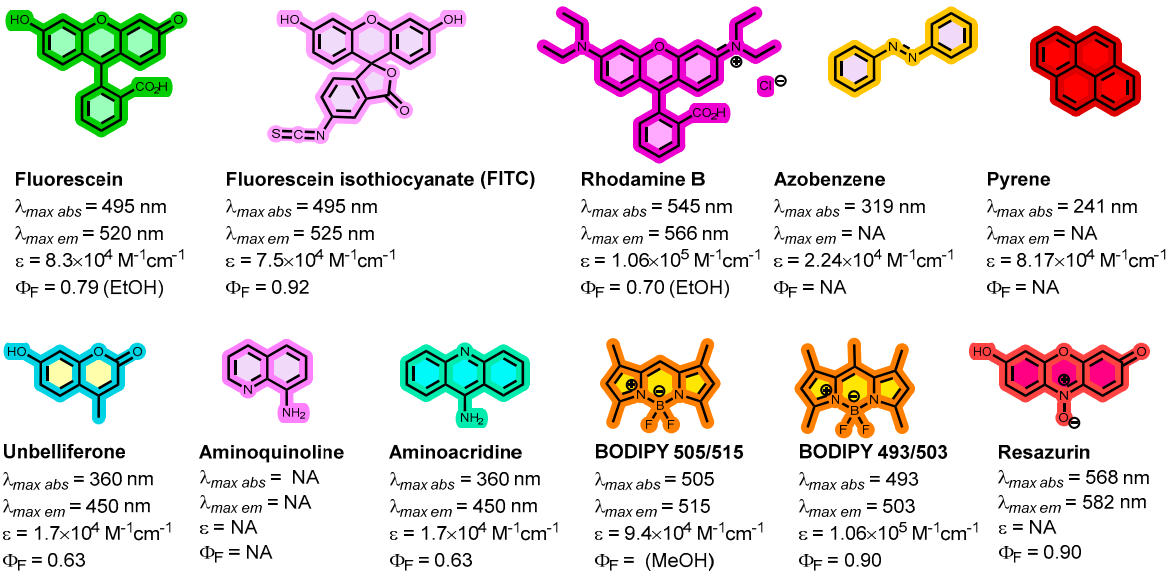

Figure 3. Structures of common fluorescent dyes.

2. Materials and Methods

2.1. Reagents and Instruments

All reactions were performed using standard laboratory equipment and glassware. All reagents and solvents used were supplied by commercial sources without further purification unless specified. All air-sensitive reactions were carried out under a nitrogen atmosphere using an oven-dried apparatus. Thin layer chromatography (TLC) was performed on Merck silica gel 60 F254 aluminium-backed plates pre-coated with silica with a thickness of 0.20 mm. Plates were visualized using either ultraviolet light of 254 nm or 365 nm or by dipping the plates into solutions of vanillin, ninhydrin, or potassium permanganate followed by heating. All column chromatography was performed under 'flash' conditions using silica gel mesh 40-63. Fourier transform infrared (FT-IR) spectra were recorded on a Perkin Elmer 100 FT-IR instrument on the neat compounds. The spectrum was processed in the software and displayed. The relevant and characteristic absorptions were reported in wavenumbers (cm^{-1}) with the intensities of the bands recorded as; broad (b), strong (s), medium (m), and weak (w). Nuclear magnetic resonance (NMR) spectroscopy was performed on Brüker Avance III 400 and 500 MHz spectrometers, where ^{1}H NMR spectra, ^{13}C NMR spectra and ^{11}B NMR were acquired at the indicated 101, 126, 128, 377 and 400 MHz as dilute solutions in the indicated deuterated solvent at ambient temperature. All spectra were recorded in deuterated dimethyl sulfoxide (DMSO-d_6), deuterated acetone (acetone-d_6) or deuterated chloroform ($CDCl_3$) obtained from Sigma Aldrich. All chemical shifts (δ) are reported in parts per million (ppm) relative to the residual protonated solvent peak (δ_H: $CHCl_3$ = 7.26 ppm, DMSO-d_6 = 2.50 ppm) or the solvent itself

 doi:10.20944/preprints202503.0093.v1

(δ_C: $CDCl_3$ = 77.0 ppm, DMSO-d_6 = 39.52 ppm). Chemical shifts (δ) were measured in parts per million (ppm) and referenced against the internal reference peaks. Coupling constants (*J*) were measured in hertz (Hz). All multiplicities are designated by the following abbreviations: s = singlet, br s = broad singlet, d = doublet, dt = doublet triplet, td = triplet doublet, ddd = doublet doublet of doublets of doublets, q = quartet, br q = broad quartet, m = multiplet. All coupling constants (*J*) are reported in Hertz (Hz). Peaks are listed in decreasing chemical shift in the following format: chemical shift (integration (^{1}H), multiplicity (^{1}H), coupling constant (^{1}H). High-resolution mass spectra were recorded using a 1260 Infinity LC (Agilent Technologies), coupled to a Quadrupole-Time of Flight tandem mass spectrometer 6530 Infinity Q-ToF detector (Agilent Technologies) by a Jet Stream ESI interface (Agilent Technologies). The LC conditions were: Zorbax Extend-C18 column (2.1 mm × 50 mm, 1.8 μm particle size); 0.4 mL/min flow rate; 1 μL injection volume for MS experiments. Separation was achieved using a gradient of water with 0.1% formic acid (eluent A) and acetonitrile with 0.1% formic acid (eluent B). The elution gradient was programmed as follows: initial conditions 5% B, followed by a linear gradient to 95% B in 15 min. The ESI operating conditions were drying gas (N_2, purity > 98%): 350 °C and 11 L/min; capillary voltage 4.0 kV; nebulizer gas 40 psig; sheath gas (N_2, purity > 98%): 375 °C and 11 L/min. High-resolution MS spectra were acquired in the positive mode in the 100–2400 m/z range. Single crystal X-ray Diffraction (SCXRD) data were collected on a Bruker D8 VENTURE diffractometer (Bruker, Karlsruhe, Germany) (Bruker AXS, Karlsruhe, Germany), equipped with a PHOTON 100 CMOS detector with graphite monochromatized Cu-Kα radiation (λ = 1.54178 Å) or a Bruker X8 Apex-II diffractometer, equipped with an Apex-II CCD area detector diffractometer (Bruker, Karlsruhe, Germany) with graphite monochromatized Mo-Kα radiation (λ = 0.71073 Å). A suitable crystal was mounted in Fomblin oil on a MiTeGen MicroLoop and cooled in a stream of cold N_2 to 100 K. Data were corrected for absorption using empirical methods (SADABS) [54–56] based upon symmetry equivalent reflections combined with measurements at different azimuthal angles. All crystal structures were solved and refined against F^2 values using ShelXT [57] for the solution and ShelXL [58] for refinement accessed via the Olex2 program [59]. All non-hydrogen atoms were refined with anisotropic displacement parameters. All hydrogen atoms were added at calculated positions and refined with a riding model and isotropic displacement parameters fixed in magnitude relative to the attached carbon atoms. Details regarding the structures and a summary table of crystallographic and data collection parameters are provided in Electronic Supplementary Information (Table S1).

2.2. Synthesis and Characterization

Synthesis of 4-(4,4,5,5-tetramethyl-1,3,2-dioxaborolan-2-yl)benzaldehyde ***2:*** Using a variation of the procedure of Miyaura et al.[60], a mixture of 4-bromobenzaldehyde (1.0 g, 5.4 mmol, 1.0 equiv.), B_2pin_2 (1.65 g, 6.5 mmol, 1.2 equiv.), KOAc (1.59 g, 16.2 mmol, 3.0 equiv.), and $PdCl_2$(dppf) (119 mg, 0.162 mmol) in dry 1,4-dioxane (20 mL) in an oven-dried two-necked round-bottom flask was degassed for 5-10 minutes using N_2 gas and stirred at 80 °C for 16 hours (overnight). Upon completion (as monitored by TLC), the reaction mixture was allowed to cool, filtered through a plug of celite, washed with EtOAc (200 mL), extracted twice with water (2 x 50 mL), and then with brine. The organic layer was dried with anhydrous $MgSO_4$, filtered, and concentrated *in vacuo*. The crude product was purified on silica gel using DCM (100 %) to obtain product **2** as a white solid (872 mg, 70% yield). ^{1}H NMR (400 MHz, $CDCl_3$) δ_H 10.02 (s, 1H, H1), 7.94 (d, *J* = 8.2 Hz, 2H, H5), 7.83 (d, *J* = 8.2 Hz, 2H, H4), 1.33 (s, 12H, H8). ^{13}C NMR (101 MHz, $CDCl_3$) δ_C 192.9 (C2), 138.4 (C3), 135.6 (C4), 129.0 (C5), 84.7 (C7), 25.2 (C8), (C6 bonded to B not observed due to broadening). LC-MS: retention time: 9.4 min; ESI-QTOF HRMS (m/z): for $[C_{13}H_{18}BO_3]^+$ $[M+H]^+$: exact mass *calcd.*: 233.1349; found: 233.1358; for $[C_{13}H_{17}BO_3Na]^+$ $[M+Na]^+$: exact mass *calcd.*: 255.1168; found: 255.1172.

1-(4-(4,4,5,5-tetramethyl-1,3,2-dioxaborolan-2-yl)phenyl)ethan-1-one ***3:*** This title compound was prepared as described above for **2** using 4-bromoacetophenone (5.0 g, 25.1 mmol, 1.0 equiv.), and B_2pin_2 (7.65 g, 30.1 mmol, 1.2 equiv.), KOAc (7.39 g, 75.3 mmol, 3.0 equiv.), $PdCl_2$(dppf) (551 mg, 0.75 mmol) in 1,4-dioxane (20 mL). The crude product was purified on silica gel using hexane/ethyl acetate

 doi:10.20944/preprints202503.0093.v1

=50:1 (*V*:*V*) to obtain product **3** as a white solid (6.15 g, 96% yield). ^{1}H NMR (500 MHz, $CDCl_3$) δ_H 7.90 (d, *J* = 6.3 Hz, 2H, H4), 7.87 (d, *J* = 6.3 Hz, 2H, H5), 2.58 (s, 3H, H1), 1.33 (s, 12H, H8). ^{13}C NMR (126 MHz, $CDCl_3$) δ_C 198.7 (C2), 139.3 (C3), 135.2 (C5), 127.6 (C4), 84.5 (C7), 27.0 (C1), 25.2 (C8), (C6 bonded to B not observed due to broadening).

2.3. Categories of Fluorescent Arylboronic Acid Chemosensor Dyes

2.3.1. Coumarin Dyes

Synthesis of 7-(diethylamino)-2H-chromen-2-one ***4****:* A mixture of 4-(diethylamino) salicylaldehyde (6.0 g, 28.69 mmol) and diethyl malonate (10.84 g, 67.75 mmol) in 90 mL anhydrous ethanol was treated with 3 mL of piperidine and then refluxed for 13 h. After removing the solvent, 120 mL of mixed solution (concentrated HCl:glacial acetic acid=1:1 (*V*:*V*)) was added to the crude product and refluxed for another 7 h. The reaction solution was poured into 300 mL of water after cooling to room temperature. The solution's pH was adjusted to 5 with NaOH. The solid was filtered and purified over silica gel (hexane: ethyl acetate=9:1 (*v*/*v*)) to give a beige solid **4** (yield: 85%). ^{1}H NMR (500 MHz, $CDCl_3$) δ_H 7.53 (d, *J* = 9.3 Hz, 1H, H9), 7.23 (d, *J* = 8.7 Hz, 1H, H5), 6.56 (dd, *J* = 8.8, 2.5 Hz, 1H, H4), 6.46 (d, *J* = 2.5 Hz, 1H, H6), 6.01 (d, *J* = 9.3 Hz, 1H, H10), 3.40 (q, *J* = 7.2 Hz, 4H, H2), 1.20 (t, *J* = 7.2 Hz, 6H, H1). ^{13}C NMR (126 MHz, $CDCl_3$) δ_C 162.4 (C11), 156.7 (C3), 150.7 (C7), 143.8 (C9), 128.8 (C5), 109.0 (C10), 108.7 (C8), 108.3 (C4), 97.4 (C6), 44.8 (C2), 12.4 (C1).

Synthesis of 7-(diethylamino)-2-oxo-2H-chromene-3-carbaldehyde ***5****:* Under N_2, anhydrous DMF (4.20 g, 57.5 mmol, 4.4 mL, 12.5 equiv.) was dropped into phosphoryl chloride ($POCl_3$) (1.76 g, 11.5 mmol, 1.1 mL, 2.5 equiv.) with stirring for 6 h in an ice bath. The solution of 7-(diethylamino)-*2H*-chromen-2-one **4** (1.00 g, 4.6 mmol, 1.0 equiv.) in anhydrous 1,2-dichloroethane (50 mL) was added to the above solution, and the mixture was stirred at 60 ℃ for 12 h. After completing the process, the mixture was poured into ice water and neutralized with NaOH solution (20%) to pH 7. The formed precipitate was filtered off and washed three times with water. The residue was chromatographed on silica, eluting with ethyl acetate/hexane (1:1, v/v) to form **5** as an orange-red solid product (yield: 79%). ^{1}H NMR (500 MHz, $CDCl_3$) δ_H 10.10 (s, 1H, H13), 8.23 (s, 1H, H9), 7.39 (d, *J* = 9.0 Hz, 1H, H5), 6.63 (dd, *J* = 9.0, 2.5 Hz, 1H, H4), 6.47 (d, *J* = 2.5 Hz, 1H, H6), 3.46 (q, *J* = 7.2 Hz, 4H, H2), 1.24 (t, *J* = 7.1 Hz, 6H, H1). ^{13}C NMR (126 MHz, $CDCl_3$) δ_C 188.0 (C12), 162.0 (C11), 159.0 (C3), 153.6 (C7), 145.5 (C9), 132.6 (C5), 114.5 (C10), 110.3 (C8), 108.4 (C4), 97.3 (C6), 45.4 (C2), 12.6 (C1). FTIR (cm^{-1}): υ (C–H st) 2879, υ(C=O st, carboxyl) 1709, υ(C=C st) 1609.

Synthesis of (E)-7-(diethylamino)-3-(3-oxo-3-(4-(4,4,5,5-tetramethyl-1,3,2-dioxaborolan-2-yl)phenyl)prop-1-en-1-yl)-2H-chromen-2-one **6**: Compound **5** (0.50 g, 2.0 mmol, 1.0 equiv.) and 1-(4-(4,4,5,5-tetramethyl-1,3,2-dioxaborolan-2-yl)phenyl)ethan-1-one **3** (0.98 g, 4.0 mmol, 2.0 equiv.) were added to 20 mL of the mixed solvent (CH_2Cl_2/anhydrous CH_3CH_2OH=1:1 (v/v)), then 10 drops of pyrrolidine were dropped into the above solution. The mixture was stirred at room temperature for 4 d, and the solvent was removed under reduced pressure. The residue was added to 40 mL of hexane/ethyl acetate (v/v=1:1) to yield red precipitations. The precipitates were collected on a filter funnel to give compound **6** as a bright red solid (yield: 51%). ^{1}H NMR (500 MHz, DMSO-d_6) δ_H 8.48 (s, 1H, H9), 8.03 (d, J = 3.2 Hz, 1H, H18), 8.00 (d, J = 4.4 Hz, 2H, H17), 7.85 (d, J = 7.7 Hz, 2H, H16), 7.67 (d, J = 15.4 Hz, 1H, H12), 7.50 (d, J = 8.9 Hz, 1H, H5), 6.80 (dd, J = 9.0, 2.4 Hz, 1H, H4), 6.60 (d, J = 2.3 Hz, 1H, H6), 3.48 (q, J = 7.1 Hz, 4H, H2), 1.32 (s, 12H, H20), 1.15 (t, J = 7.0 Hz, 6H, H1). ^{13}C NMR (126 MHz, DMSO-d_6) δ_C 189.1 (C14), 160.0 (C11), 156.5 (C3), 152.0 (C7), 146.0 (C12), 140.0 (C9), 139.9 (C15), 134.8 (C17), 130.7 (C5), 127.4 (C16), 120.7 (C10), 113.1 (C13), 110.0 (C8), 108.4 (C4), 96.3 (C6), 84.1 (C19), 44.3 (C2), 24.7 (C20), 12.4 (C1), (C18 bonded to B not observed due to broadening).

(E)-(4-(3-(7-(diethylamino)-2-oxo-2H-chromen-3-yl)acryloyl)phenyl)boronic acid ***7****:* Deprotection of pinacol boronate esters was performed according to the procedure by Akgun [61]. (*E*)-7-(diethylamino)-3-(3-oxo-3-(4-(4,4,5,5-tetramethyl-1,3,2-dioxaborolan-2-yl)phenyl)prop-1-en-1-yl)-*2H*-chromen-2-one **6** (150 mg, 0.36 mmol, 1.0 equiv.) was dissolved in THF: water (4:1 mL) (4:1 v/v). Then sodium periodate (231 mg, 1.08 mmol, 3.0 equiv.) was added to the solution and stirred at room

 doi:10.20944/preprints202503.0093.v1

temperature for 30 min under an ambient atmosphere. Lastly, HCl (0.2 mL, 1 N) was added to the reaction mixture, which was stirred for 24 h at room temperature. The reaction mixture was concentrated *in vacuo*. Then it was dissolved in EtOAc (30 mL) and washed with water (1 × 8 mL), and brine (1 × 8 mL). The organic fraction was dried ($MgSO_4$), filtered and concentrated *in vacuo* to obtain pure (*E*)-(4-(3-(7-(diethylamino)-2-oxo-*2H*-chromen-3-yl)acryloyl)phenyl)boronic acid **7** (yield: 90%). ^{1}H NMR (400 MHz, DMSO-*d*$_6$) δ_H 8.47 (s, 1H, H9), 8.29 (s, 2H, H19), 8.06 (d, *J* = 19.8 Hz, 1H, H5), 8.00 – 7.95 (m, 4H, H16, H17), 7.66 (d, *J* = 15.4 Hz, 1H, H12), 7.48 (d, *J* = 9.0 Hz, 1H, H13), 6.78 (dd, *J* = 9.0, 2.4 Hz, 1H, H4), 6.59 (d, *J* = 2.4 Hz, 1H, H6), 3.47 (q, *J* = 7.0 Hz, 4H, H2), 1.14 (t, *J* = 7.0 Hz, 6H, H1). ^{13}C NMR (101 MHz, DMSO-*d*$_6$) δ_C 189.2 (C14), 160.0 (C11), 156.5 (C3, 151.9 (C7), 145.5 (C12), 139.4 (C9), 139.0 (C15), 134.4 (C17), 130.7 (C5), 127.0 (C16), 120.9 (C10), 113.2 (C13), 109.9 (C8), 108.4 (C4), 96.3 (C6), 44.3 (C2), 12.4 (C1), (C18 bonded to B not observed due to broadening). ^{11}B NMR (128 MHz, DMSO-*d*$_6$) δ_B 28.4. LC-MS: retention time: 8.8 min; ESI-QTOF HRMS (m/z): for $[C_{22}H_{23}BNO_5]^+$ $[M+H]^+$: exact mass *calcd.*: 392.1669; found: 392.1680. FTIR (cm^{-1}): υ(O–H st) 3378, υ(C–H st) 2974, υ(C=O st, carboxyl) 1719, υ(C=C st) 1560.

(4-(((4-methyl-2-oxo-2H-chromen-7-yl)oxy)methyl)phenyl)boronic acid **22***:* 4-Bromomethylphenylboronic acid (297 mg, 1.0 mmol) and 4-methylumbelliferone (4-MU) (194 mg, 1.1 mmol) were dissolved in 5 mL dry dimethylformamide (DMF). Cesium chloride (360 mg, 1.1 mmol) was then added and stirred at 70 °C for 1.5 h. The solution was extracted using CH_2Cl_2 and deionized water after the mixture was cooled to room temperature. The organic layer was collected, dried over anhydrous magnesium sulfate, and concentrated. The crude material was purified using a silica column (hexane: ethyl acetate =5:3) to afford **22** as a white solid (298 mg, 76%). ^{1}H NMR (400 MHz, DMSO-*d*$_6$) δ_H 8.06 (s, 2H, H16), 7.81 (d, *J* = 7.8 Hz, 2H, H14), 7.67 (d, *J* = 8.6 Hz, 1H, H9), 7.42 (d, *J* = 8.0 Hz, 2H, H13), 7.06 – 7.01 (m, 2H, H6, H7), 6.20 (d, *J* = 1.4 Hz, 1H, H2), 5.23 (s, 2H, H11), 2.38 (d, *J* = 1.3 Hz, 3H, H4). ^{13}C NMR (101 MHz, DMSO-*d*$_6$) δ_C 161.3 (C8), 160.1 (C1), 154.7 (C10), 153.4 (C3), 138.0 (C12), 134.3 (C14), 126.7 (C13), 126.5 (C6), 113.3 (C5), 112.7 (C2), 111.2 (C7), 101.7 (C9), 69.8 (C11), 18.1 (C4), (C15 bonded to B not observed due to broadening). ^{11}B NMR (128 MHz, DMSO-*d*$_6$) δ_B 28.9. LC-MS: retention time: 7.5 min; ESI-QTOF HRMS (m/z): for $[C_{17}H_{16}BO_5]^+$ $[M+H]^+$: exact mass *calcd.*: 311.1091; found: 311.1096. FTIR (cm^{-1}): υ(N–H st) 3328, υ(O–H st) 3224, υ(C–H st) 2938, υ(C=O st, carboxyl) 1691, υ(C=C st) 1604.

2.3.2. 9-Aminoacridine Dyes

Synthesis of N-(acridin-9-yl)-2-chloroacetamide ***23****:* Chloroacetyl chloride (1.15 g, 10.2 mmol, 0.8 mL, 2.0 equiv.) in THF (20 mL) was added dropwise while stirring to a mixture of 9-aminoacridine (1.00 g, 4.0 mmol, 1.0 equiv.) and TEA (1.03 g, 10.2 mmol, 1.4 mL, 2.0 equiv.) in THF at 0 – 5 °C. The reaction mixture was then stirred for 4 h. The solvent was evaporated under reduced pressure. The residue was washed with water to remove TEA.HCl before being dried and recrystallized from ethanol to obtain **23** (yield: 59%). ^{1}H NMR (400 MHz, DMSO-*d*$_6$) δ_H 12.19 (s, 1H, H9), 8.48 (d, 4H, H3), 8.23 (dd, *J* = 9.0, 6.5 Hz, 2H, H1), 7.87 (dd, 2H, H2), 4.84 (s, 2H, H11). ^{13}C NMR (101 MHz, DMSO-*d*$_6$) δ_C 166.6 (C10), 141.5 (C6, C8), 135.8 (C5, C7), 126.9 (C3), 125.9 (C1), 121.4 (C2), 43.2 (C11). LC-MS: retention time: 4.7 min; ESI-QTOF HRMS (m/z): for $[C_{15}H_{12}ClN_2O]^+$ $[M+H]^+$: exact mass *calcd.*: 271.0638; found: 271.0750.

(4-(((2-(acridin-9-ylamino)-2-oxoethyl)amino)methyl)phenyl)boronic acid ***24****: N*-(acridin-9-yl)-2-chloroacetamide **23** (536 mg, 1.98 mmol, 1.1 equiv.), (4-(aminomethyl)phenyl)boronic acid (270 mg, 1.80 mmol, 1.0 equiv.), and triethylamine (TEA, 0.5 mL, 3.60 mmol, 2.0 equiv.) were dissolved in acetonitrile (MeCN, 30 mL), stirred, and refluxed for 1 d. The oily residue was dissolved in methylene chloride and washed five times with 10 mL of water. The organic layer was dried over anhydrous Na_2SO_4. The solvent was removed under reduced pressure to obtain the crude product, which was purified by silica gel column chromatography (Hexanes: EtOAc - 9:1) (yield: 22%). ^{1}H NMR (400 MHz, DMSO-*d*$_6$) δ_H 9.56 (s, 1H, H8), 9.24 (s, 1H, H11), 7.91 (s, 2H, H17), 7.58 (d, *J* = 7.9 Hz, 2H, H14), 7.49 (dd, *J* = 7.9, 1.5 Hz, 2H, H2), 7.28 (ddd, *J* = 8.3, 5.8, 1.5 Hz, 2H, H3), 7.02 – 6.95 (m, 4H, H1, H4), 6.90 (d, *J* = 7.7 Hz, 2H, H15), 3.23 (s, 2H, H12), 2.95 (s, 2H, H10). ^{13}C NMR (101 MHz, DMSO-*d*$_6$) δ_C

 doi:10.20944/preprints202503.0093.v1

171.4 (C9), 140.3 (C5), 138.6 (C7), 134.0 (C13), 128.7 (C15), 128.0 (C3), 126.6 (C14), 119.5 (C1), 119.1 (C2), 114.9 (C6), 114.1 (C4), 53.3 (C12), 52.1 (C10), (C16 bonded to B not observed due to broadening). ^{11}B NMR (128 MHz, DMSO-d_6) δ_B 29.18. LC-MS: retention time: 0.5 min; ESI-QTOF HRMS (m/z): for $[C_{22}H_{21}BN_3O_3]^+$ $[M+H]^+$: exact mass *calcd.*: 386.1676; found: 386.1683. FTIR (cm^{-1}): υ(N–H st) 3328, υ(C-H st, carboxyl) 2976, υ(C=O st, amide) 1673, υ(C=C st and C=N st) 1613–1477.

2.3.3. 8-Aminoquinoline Dyes

Synthesis of 2-(tert-butoxycarbonylamino)acetic acid 25: Based on the procedure adopted from Ear et al [62], Glycine (10.0 g, 133.2 mmol, 1.0 equiv.) was dissolved in a dioxane-water (1:1) (200 mL) mixture. Triethylamine (18.5 mL, 133.2 mmol, 1.0 equiv.) and di-*tert*-butyl dicarbonate (*Boc*$_2$O, 31.98 g, 146.5 mmol, 1.1 equiv.) were added and the mixture was stirred for 2 h at room temperature. After evaporation of the volatiles, redissolving in water/diethyl ether (150 mL/250 mL) for extraction. The aqueous phase was recovered, and the pH was adjusted to 2 with a 2 M solution of HCl. The mixture was extracted with ethyl acetate (2 x 150 mL), dried over $MgSO_4$, and concentrated in vacuo, to yield white crystalline product **25**, yield (15.08 g, 65% yield). The data were consistent with the literature [62]. ^{1}H NMR (400 MHz, DMSO-d_6) δ_H 7.05 (t, J = 6.2 Hz, 1H, H4), 3.57 (d, J = 6.2 Hz, 2H, H5), 1.38 (s, 9H, H1). ^{13}C NMR (101 MHz, DMSO-d_6) δ_C 171.8 (C6), 155.9 (C3), 78.1 (C2), 41.8 (C5), 28.2 (C1). LC-MS: retention time: 4.7 min; ESI-QTOF HRMS (m/z): for $[C_{14}H_{17}BNO_2]^+$ $[M+H]^+$: exact mass calcd.: 198.0742; found: 198.0756.

Synthesis of tert-butyl (2-oxo-2-(quinolin-8-ylamino)ethyl)carbamate ***26****:* A mixture of 8-aminoquinoline (2.56 g, 17.7 mmol, 1.0 equiv.), DMAP (108 mg, 5 mol%) and *Boc*-Gly-OH, **25** (1.22 g, 6.94 mmol, 2.0 equiv.) in dichloromethane (100 mL) were stirred in an ice bath (~0 °C) for 30 minutes, followed by an addition of EDC·HCl (1.33 g, 6.94 mmol, 2.0 equiv.). The reaction mixture was stirred at 0 °C for 2 hours and stirred overnight at room temperature. The crude was extracted with NH_4Cl (aq.) (100 mL). The organic layer was dried over $MgSO_4$, filtered, and concentrated under a vacuum. The crude product was purified through silica-gel column chromatography using hexane/ethyl acetate (3:2) as an eluent to afford tert-butyl (2-oxo-2-(quinolin-8-ylamino)ethyl)carbamate **26** as a white solid (4.95 g, 93% yield). The data were consistent with the literature [63]. ^{1}H NMR (500 MHz, $CDCl_3$) δ_H 10.26 (s, 1H, H10), 8.74 (d, *J* = 4.2 Hz, 1H, H1), 8.70 (dd, *J* = 6.3, 2.7 Hz, 1H, H3), 8.10 (d, *J* = 8.3 Hz, 1H, H7), 7.48 (d, *J* = 8.4 Hz, 1H, H5), 7.46 (s, 1H, H2), 7.40 (dd, *J* = 8.3, 4.2 Hz, 1H, H6), 5.51 (s, 1H, H13), 4.11 (d, *J* = 5.9 Hz, 2H, H12), 1.50 (s, 9H, H16). ^{13}C NMR (126 MHz, $CDCl_3$) δ_C 168.1 (C11), 156.1 (C14), 148.3 (C1), 138.4 (C9), 136.4 (C8), 133.9 (C3), 128.0 (C4), 127.3 (C6), 122.0 (C2), 121.7 (C5), 116.8 (C7), 80.3 (C15), 45.4 (C12), 28.4 (C16). LC-MS: retention time: 8.0 min; ESI-QTOF HRMS (m/z): for $[C_{16}H_{20}N_3O_3]^+$ $[M+H]^+$: exact mass *calcd.*: 302.1505; found: 302.1523.

Boc deprotection of tert-butyl (2-oxo-2-(quinolin-8-ylamino)ethyl)carbamate ***27:*** Based on the procedure by Ear *et al*, *tert*-butyl (2-oxo-2-(quinolin-8-ylamino)ethyl)carbamate **26** (3.00 g, 9.96 mmol, 1.0 equiv.) was dissolved in CH_2CI_2 (150 mL) and HCI-dioxane (4 M solution, 20 mL) was added and the mixture was stirred at rt overnight. The reaction was monitored by TLC. After completion of the reaction, the solvents were removed *in vacuo* to obtain the hydrochloride salt of the amine. The residue was dissolved in diethyl ether and extracted with NaOH (2 M) and Et_2O. the organic layer was dried over $MgSO_4$ and the solvent was evaporated under reduced pressure to obtain the product 2-amino-*N*-(quinolin-8-yl)acetamide **27** (1.68 g, 84% yield). ^{1}H NMR (500 MHz, $CDCl_3$) δ_H 11.25 (s, 1H, H10), 8.85 (d, 1H, H1), 8.82 (dd, 1H, H3), 8.14 (d, 1H, H7), 7.56 – 7.47 (m, 2H, H2, H5), 7.43 (dd, *J* = 8.3, 4.2 Hz, 1H, H6), 3.64 (s, 2H, H13), 1.81 (s, 2H, H12). ^{13}C NMR (126 MHz, $CDCl_3$) δ_C 171.9 (C11), 148.9 (C1), 139.3 (C9), 136.6 (C8), 134.6 (C3), 128.4 (C4), 127.7 (C6), 122.1 (C2), 121.9 (C5), 116.9 (C7), 46.5 (C12). LC-MS: retention time: 1.1 min; ESI-QTOF HRMS (m/z): for $[C_{11}H_{12}N_3O]^+$ $[M+H]^+$: exact mass *calcd.*: 202.0980; found: 202.0997; for $[C_{11}H_{11}N_3ONa]^+$ $[M+Na]^+$: exact mass *calcd.*: 224.0800; found: 224.0804.

Synthesis of N-(quinolin-8-yl)-2-((4-(4,4,5,5-tetramethyl-1,3,2-dioxaborolan-2-yl)benzyl)amino)acetamide ***28****:* 2-amino-*N*-(quinolin-8-yl)acetamide **27** (0.82 g, 4.07 mmol, 1.2 equiv.) and 4-(4,4,5,5-tetramethyl-1,3,2-dioxaborolan-2-yl)benzaldehyde **2** (0.79 g, 3.39 mmol, 1.0 equiv.)

 doi:10.20944/preprints202503.0093.v1

were dissolved in 1, 2-dichloroethane (50 mL). The reaction mixture was then charged with sodium triacetoxyborohydride (1.08 g, 1.5 equiv.). The reaction was then stirred under nitrogen for 1 h. After an hour, additional sodium triacetoxyborohydride (0.75 g, 1.0 equiv.) was added to the reaction and the mixture was stirred for a further 1 h. The reaction mixture was then quenched with saturated $NaHCO_3$ solution (100 mL). The aqueous phase was extracted with CH_2Cl_2 (2 x 100 mL), and the combined organics dried over anhydrous $MgSO_4$ and concentrated to dryness *in vacuo* to afford *N*-(quinolin-8-yl)-2-((4-(4,4,5,5-tetramethyl-1,3,2-dioxaborolan-2-yl)benzyl)amino)acetamide **28** as a white solid (0.75 g, 53% yield). ^{1}H NMR (400 MHz, $CDCl_3$) δ_H 11.61 (s, 1H, H10), 8.92 (dd, *J* = 4.2, 1.7 Hz, 1H, H1), 8.82 (dd, *J* = 7.0, 2.0 Hz, 1H, H3), 8.17 (d, *J* = 8.2 Hz, 1H, H7), 7.83 (d, *J* = 7.4 Hz, 2H, H17), 7.62 (d, *J* = 7.8 Hz, 2H, H16), 7.59 – 7.49 (m, 2H, H2, H5), 7.48 (dd, *J* = 8.3, 4.3 Hz, 1H, H6), 3.94 (s, 2H, H14), 3.61 (s, 2H, H12), 1.36 (s, 12H, H20). ^{13}C NMR (101 MHz, $CDCl_3$) δ_C 170.4 (C11), 148.6 (C1), 142.8 (C9), 139.1 (C15), 136.3 (C8), 135.2 (C17), 134.5 (C3), 128.2 (C4), 128.0 (C16), 127.5 (C6), 121.8 (C2), 121.7 (C5), 116.6 (C7), 83.9 (C19), 54.4 (C14), 53.4 (C12), 25.0 (C20), (C18 bonded to B not observed due to broadening). ^{11}B NMR (128 MHz, $CDCl_3$) δ_B 31.6. LC-MS: retention time: 6.9 min; ESI-QTOF HRMS (m/z): for $[C_{24}H_{29}BN_3O_3]^+$ [M+H]$^+$: exact mass *calcd.*: 418.2302; found: 418.2320; for $[C_{24}H_{28}BN_3O_3Na]^+$ [M+Na]$^+$: exact mass *calcd.*: 440.2121; found: 440.2123.

(4-(((2-oxo-2-(quinolin-8-ylamino)ethyl)amino)methyl)phenyl)boronic acid ***29:*** Deprotection of pinacol boronate esters was performed according to the procedure by Akgun [61]. The title compound was prepared as described above for **7.** *N*-(quinolin-8-yl)-2-((4-(4,4,5,5-tetramethyl-1,3,2-dioxaborolan-2-yl)benzyl)amino)acetamide **28** (150 mg, 0.36 mmol, 1.0 equiv.) was dissolved in THF: water (4:1 mL) (4:1 v/v). Then, sodium periodate (231 mg, 1.08 mmol, 3.0 equiv.) was added to the solution and stirred at room temperature for 30 min under an ambient atmosphere. Lastly, HCl (0.2 mL, 1 N) was added to the reaction mixture, which was stirred for 24 h at room temperature. The reaction mixture was concentrated *in vacuo*. Then it was dissolved in EtOAc (30 mL) and washed with water (1 × 8 mL), and brine (1 × 8 mL). The organic fraction was dried ($MgSO_4$), filtered and concentrated *in vacuo* to obtain pure (4-(((2-oxo-2-(quinolin-8-ylamino)ethyl)amino)methyl)phenyl)boronic acid **29** as a white solid (yield: 76%). ^{1}H NMR (400 MHz, DMSO-d_6) δ_H 11.62 (s, 1H, H10), 8.98 (dd, *J* = 4.2, 1.7 Hz, 1H, H1), 8.71 (dd, *J* = 7.6, 1.4 Hz, 1H, H3), 8.43 (dd, *J* = 8.3, 1.7 Hz, 1H, H7), 8.00 (s, 2H, H19), 7.78 (d, *J* = 8.0 Hz, 2H, H17), 7.69 – 7.68 (m, 1H, H13), 7.66 (dd, *J* = 2.7, 1.4 Hz, 1H, H6), 7.62 – 7.57 (m, 2H, H2, H6), 7.53 (d, *J* = 7.9 Hz, 2H, H16), 3.82 (s, 2H, H14), 3.40 (s, 2H, H12). ^{13}C NMR (101 MHz, DMSO-d_6) δ_C 170.5 (C11), 149.0 (C1), 138.1 (C9), 136.6 (C15), 134.2 (C8), 134.1 (C17), 133.9 (C3), 127.9 (C4), 127.4 (C16), 127.1 (C6), 122.3 (C2), 121.7 (C5), 115.4 (C7), 53.2 (C14), 52.6 (C12). ^{11}B NMR (128 MHz, DMSO-d_6) δ_B 29.09. LC-MS: retention time: 5.2 min; ESI-QTOF HRMS (m/z): for $[C_{18}H_{19}BN_3O_3]^+$ [M+H]$^+$: exact mass *calcd.*: 336.1519; found: 336.1524. FTIR (cm^{-1}): υ (O–H st) 3265, υ(C–H st) 2829, υ(C=O st, amide) 1669, υ(C=C st and C=N st) 1604–1524.

2.3.4. Fluorescein Dyes

Synthesis of fluorescein methyl ester ***34:*** To fluorescein (1.0 g, 3.1 mmol) methanol solution (10 mL) in a 50 mL round-bottom flask, was added concentrated sulfuric acid (98%) (1 mL). The solution was refluxed and stirred for 4 h. After cooling, excess methanol was removed under reduced pressure and excess water was added to the residue. The red solid formed was washed with water several times and filtered in a vacuum until almost free from fluorescence. After drying in a vacuum, the crude product was redissolved and columned using CH_2Cl_2: methanol (10:1) to obtain red solid fluorescein methyl ester **34** (93% yield). ^{1}H NMR (400 MHz, DMSO-d_6) δ_H 8.31 (dd, *J* = 7.8, 1.3 Hz, 1H, H18), 7.96 (td, *J* = 7.5, 1.4 Hz, 1H, H16), 7.88 (td, *J* = 7.7, 1.4 Hz, 1H, H17), 7.55 (dd, *J* = 7.5, 1.4 Hz, 1H, H15), 7.31 (d, *J* = 9.2 Hz, 2H, H6, H10), 7.24 (d, *J* = 2.2 Hz, 2H, H2, H12), 7.10 (dd, *J* = 9.2, 2.2 Hz, 2H, H3, H13), 3.57 (s, 3H, H21). ^{13}C NMR (101 MHz, DMSO-d_6) δ_C 171.5, 165.0, 158.1, 133.3, 133.1, 132.3, 130.9, 130.3, 129.1, 120.7, 116.0, 102.5, 52.6. LC-MS: retention time: 6.8 min; ESI-QTOF HRMS (m/z): for $[C_{21}H_{15}O_5]^+$ [M+H]$^+$: exact mass *calcd.*: 347.0920; found: 347.0934.

 doi:10.20944/preprints202503.0093.v1

Synthesis of fluorescein hydrazide ***35:*** Fluorescein methyl ester **34** (0.40 g) and hydrazine hydrate (0.24 g, 4.8 mmol) were added to methanol (5 mL), refluxed, and stirred for 6 h. After collecting by filtration, the light brown precipitate was washed with a small amount of methanol and water and dried in a vacuum to obtain the crude product. The crude material was pre-adsorbed onto silica and purified by column chromatography using CH_2Cl_2: MeOH (10:1) to obtain pure straw yellow fluorescein hydrazide **35** (96% yield). ^{1}H NMR (400 MHz, DMSO-d_6) δ_H 9.80 (s, 2H, H22), 7.77 (ddd, J = 5.2, 2.4, 0.8 Hz, 1H, H18), 7.50 – 7.47 (m, 2H, H16, H17), 7.00 – 6.98 (m, 1H, H15), 6.59 (d, J = 2.3 Hz, 2H, H6, H10), 6.45 (dd, J = 8.6, 2.4 Hz, 2H, H2, H12), 6.40 (d, J = 8.6 Hz, 2H, H3, H13), 4.38 (s, 2H, H21). ^{13}C NMR (101 MHz, DMSO-d_6) δ_C 165.5, 158.2, 152.4, 151.5, 132.6, 129.3, 128.4, 128.0, 123.4, 122.4, 112.0, 110.0, 102.4, 64.6. LC-MS: retention time: 6.5 min; ESI-QTOF HRMS (m/z): for $[C_{20}H_{15}N_2O_4]^+$ $[M+H]^+$: exact mass *calcd.*: 347.1032; found: 347.1028.

(E)-(4-(((3′,6′-dihydroxy-3-oxospiro[isoindoline-1,9′-xanthen]-2-yl)imino)methyl)phenyl)boronic acid ***36:*** 4-formylphenylboronic acid (0.391 mL, 1.77 mmol) was dissolved in 20 mL of a mixture of ethanol/toluene (90:10) and then **35** (0.200 g, 0.578 mmol) was added. A Dean-Stark trap was fixed to the reaction vessel and filled with 10 mL of the same solvent mixture for the azeotropic removal of water. The reaction was then allowed to stir for 16 h at 100 °C at which time TLC showed that the starting material had fully reacted. The solvent was removed under vacuum, and the product was recrystallized to obtain the product **36** (64% yield). ^{1}H NMR (400 MHz, DMSO-d_6) δ_H 9.92 (s, 2H, H27), 8.96 (s, 1H, H21), 8.10 (s, 2H, H26), 7.92 (d, J = 7.3 Hz, 1H, H18), 7.75 (d, J = 7.9 Hz, 2H, H24), 7.68 – 7.55 (m, 2H, H16, H17), 7.38 (d, J = 8.0 Hz, 2H, H23), 7.14 (d, J = 7.4 Hz, 1H, H15), 6.67 (d, J = 2.2 Hz, 2H, H6, H10), 6.51 (d, J = 8.6 Hz, 2H, H2, H12), 6.46 (dd, J = 8.6, 2.3 Hz, 2H, H). ^{13}C NMR (101 MHz, DMSO-d_6) δ_C 163.7, 158.6, 152.2, 150.5, 148.9, 135.8, 134.5, 134.1, 129.1, 128.9, 128.0, 125.7, 123.8, 123.2, 112.4, 110.1, 102.5, 65.3. ^{11}B NMR (128 MHz, DMSO-d_6) δ_B 28.1. LC-MS: retention time: 7.4 min; ESI-QTOF HRMS (m/z): for $[C_{27}H_{20}BN_2O_6]^+$ $[M+H]^+$: exact mass *calcd.*: 479.1414; found: 479.1412. FTIR (cm^{-1}): υ (O–H st) 3287, υ(C=O st, amide) 1668, υ(C=C st and C=N st) 1600–1318.

3-(3-(3′,6′-Dihydroxy-3-oxo-3H-spiro[isobenzofuran-1,9′-xanthene]-5-yl)thioureido)phenylboronic acid ***37:*** 3-Aminobenzeneboronic acid (0.35 g, 2.57 mmol) was added to a solution of fluorescein isothiocyanate isomer I (1.00 g, 2.57 mmol) in DMF (5 mL). The reaction mixture was stirred at room temperature for 12 h and then poured into methanol (10 mL). The solvents were removed *in vacuo* the residue was then dissolved in the minimum amount of fresh methanol. Chloroform was added and product **37** was obtained as a bright orange precipitate (920 mg, 68% yield). LC-MS: retention time: 7.0 min; ESI-QTOF HRMS (m/z): for $[C_{27}H_{20}BN_2O_7S]^+$ $[M+H]^+$: exact mass *calcd.*: 527.1084; found: 527.1123.

2.3.5. Rhodamine Dyes

Synthesis of rhodamine B hydrazide ***38:*** To 0.4 g of rhodamine B (I) dissolved in 15 ml of methanol, an excessive hydrazine hydrate (0.5 ml) was added and then the reaction solution was refluxed till the pink colour disappeared. After that, the cooled reaction solution was poured into distilled water and extracted with ethyl acetate (6 × 25 ml). The combined extracts were dried with sodium sulfate anhydrous and filtered, and the solvent was evaporated to obtain rhodamine B hydrazide **38** in 68% yield. ^{1}H NMR (400 MHz, DMSO-d_6) δ_H 7.79 – 7.73 (m, 1H, H12), 7.50 – 7.43 (m, 2H, H10, H11), 7.01 – 6.95 (m, 1H, H9), 6.37 (t, J = 1.4 Hz, 2H, H2), 6.33 (d, J = 1.4 Hz, 4H, H3, H6), 4.26 (s, 2H, H15), 3.31 (q, 8H, H16), 1.08 (t, J = 7.0 Hz, 12H, H17). ^{13}C NMR (101 MHz, DMSO-d_6) δ_C 165.3 (C14), 153.0 (C5), 151.9 (C1), 148.1 (C8), 132.4 (C10), 129.6 (C13), 128.1 (C11), 127.7 (C3), 123.5 (C9), 122.1 (C12), 107.8 (C4), 105.5 (C2), 97.4 (C6), 64.8 (C7), 43.7 (C16), 12.5 (C17). LC-MS: retention time: 8.6 min; ESI-QTOF HRMS (m/z): for $[C_{28}H_{33}N_4O_2]^+$ $[M+H]^+$: exact mass *calcd.*: 457.2604; found: 457.2596.

(E)-(4-(((2-(3′,6′-bis(diethylamino)-3-oxospiro[isoindoline-1,9′-xanthen]-2-yl)ethyl)imino)methyl)phenyl)boronic acid ***39:*** 4-formylphenylboronic acid (0.391 mL, 1.77 mmol) was dissolved in 20 mL of a mixture of ethanol/toluene (90:10) and then **38** (0.200 g, 0.578 mmol) was added. A Dean-Stark trap was fixed to the reaction vessel and filled with 10 mL of the same solvent mixture for the azeotropic removal of water. The reaction was then allowed to stir for 16 h at 100 °C

 doi:10.20944/preprints202503.0093.v1

at which time TLC showed that the starting material **38** had fully reacted. The solvent was removed under vacuum, and the product was recrystallized to obtain product **39** (73% yield). ^{1}H NMR (400 MHz, $CDCl_3$) δ_H 8.07 (d, *J* = 7.8 Hz, 1H, H12), 8.00 (d, *J* = 6.4 Hz, 1H, H10), 7.74 (d, *J* = 7.8 Hz, 1H, H11), 7.65 – 7.62 (m, 3H, H9, H20), 7.56 – 7.53 (d, *J* = 7.1 Hz, 2H, H18), 7.47 (d, *J* = 7.1 Hz, 2H, H17), 7.14 – 7.09 (m, 1H, H15), 6.52 (dd, *J* = 8.9, 6.5 Hz, 2H, H2), 6.46 (dd, *J* = 14.9, 2.6 Hz, 2H, H3), 6.24 (ddd, *J* = 9.1, 7.2, 2.6 Hz, 2H, H6), 3.31 (q, *J* = 9.0, 8.1 Hz, 8H, H16), 1.15 (t, *J* = 6.6 Hz, 12H, H17). ^{13}C NMR (101 MHz, $CDCl_3$) δ_C 165.3, 153.4, 153.2, 152.0, 149.1, 149.1, 147.1, 137.5, 135.63, 134.0, 133.6, 133.4, 128.4, 128.1, 127.0, 124.0, 123.6, 108.2, 106.0, 98.0, 58.6, 44.5, 12.7. ^{11}B NMR (128 MHz, $CDCl_3$) δ_B 29.9. LC-MS: retention time: 10.2 min; ESI-QTOF HRMS (m/z): for $[C_{35}H_{38}BN_4O_4]^+$ $[M+H]^+$: exact mass *calcd.*: 589.2986; found: 589.2994. FTIR (cm^{-1}): υ (O–H st) 3310, υ(C–H st) 2893, υ(C=O st, amide) 1696, υ(C=C st and C=N st) 1614–1306.

2.3.6. BODIPY Dyes

*Synthesis of protected BODIPY dye **42**:* A mixture of a protected 4-formylphenylboronic acid **2** (1.50 g, 6.5 mmol, 1.0 equiv.) and 2,4-dimethyl-*1H*-pyrrole (1.24 g, 13.0 mmol, 2.0 equiv.) was dissolved in anhydrous DCM (40 mL) under nitrogen. TFA (0.4 mL) was added to the mixture and stirred at room temperature for 3 h. The consumption of the aldehyde was monitored by TLC. A solution of *p*-chloranil in DCM (1.92 g, 7.8 mmol, 1.2 equiv.) was added at 0 °C and stirred for 30 min. TEA (3.95 g, 5.4 mL, 39.0 mmol, 6.0 equiv.) was added at 0 °C and stirred for a further 30 min. Thereafter, $BF_3{\cdot}OEt_2$ (9.23 g, 8.0 mL, 65.0 mmol, 10.0 equiv.) was added dropwise, and the reaction was stirred for 12 h at room temperature. The mixture was evaporated under reduced pressure to obtain the crude product. The crude product was purified by silica gel column using hexane/ethyl acetate (1:0→ 9:1) to obtain the desired product **42** in 47% yield. ^{1}H NMR (500 MHz, $CDCl_3$) δ_H 7.90 (d, *J* = 7.5 Hz, 2H, H10), 7.29 (d, *J* = 7.5 Hz, 2H, H9), 5.97 (s, 2H, H3), 2.55 (s, 6H, H6), 1.38 (s, 12H, H13), 1.36 (s, 6H, H7). ^{13}C NMR (126 MHz, $CDCl_3$) δ_C 155.6 (C4), 143.4 (C1), 141.8 (C2), 138.0 (C8), 135.5 (C10), 131.4 (C5), 127.5 (C9), 121.3 (C3), 84.3 (C12), 29.8 (C7), 25.1 (C13), 14.7 (C6), (C11 bonded to B not observed due to broadening). LC-MS: retention time: 12.4 min; ESI-QTOF HRMS (m/z): for $[C_{25}H_{31}B_2F_2N_2O_2]^+$ $[M+H]^+$: exact mass *calcd.*: 451.2540; found: 451.2555.

*Deprotection of protected BODIPY dye **42** to obtain **45**:* Deprotection of pinacol boronate esters was performed according to the procedure by Akgun [61]. BODIPY dye **42** (150 mg, 0.36 mmol, 1.0 equiv.) was dissolved in THF: water (4:1 mL) (4:1 v/v). Then sodium periodate (231 mg, 1.08 mmol, 3.0 equiv.) was added to the solution and stirred at room temperature for 30 min under an ambient atmosphere. Lastly, HCl (0.2 mL, 1 N) was added to the reaction mixture, which was stirred for 24 h at room temperature. The reaction mixture was concentrated *in vacuo*. Then it was dissolved in EtOAc (30 mL) and washed with water (1 × 8 mL), and brine (1 × 8 mL). The organic fraction was dried ($MgSO_4$), and the solids were removed by gravity filtration. The crude product was preabsorbed onto 5 mL of silica and dried under vacuum. Flash chromatography (1:3 hexanes/EtOAc) provided a pure deprotected BODIPY dye **45** (89% yield) as a reddish-orange powder after solvent removal. ^{1}H NMR (400 MHz, DMSO-d_6) δ_H 8.25 (s, 2H, H12), 7.96 (d, *J* = 7.9 Hz, 2H, H10), 7.33 (d, *J* = 7.9 Hz, 2H, H9), 6.17 (s, 2H, H3), 2.44 (s, 6H, H6), 1.32 (s, 6H, H7). ^{13}C NMR (101 MHz, DMSO-d_6) δ_C 154.8, 150.9, 142.8, 142.2, 135.7, 134.9, 130.6, 129.2, 126.7, 121.4, 113.8, 101.6, 14.3, 14.0. LC-MS: retention time: 9.0 min; ESI-QTOF HRMS (m/z): for $[C_{19}H_{21}B_2F_2N_2O_2]^+$ $[M+H]^+$: exact mass *calcd.*: 369.1757; found: 369.1763. FTIR (cm^{-1}): υ (O–H st) 3201, υ(C–H st) 2916, υ(C=C st and C=N st) 1545–1454.

2.3.7. Azo Dyes

*Synthesis of (2-((m-tolylamino)methyl)phenyl)boronic acid **46**:* 2-formylbenzeneboronic acid (3.00 g, 20.1 mmol, 1.0 equiv.) and m-toluidine (2.7 mL, 24.1 mmol, 1.1 equiv.) were dissolved in 1, 2-dichloroethane (50 mL). The reaction mixture was then charged with sodium triacetoxyborohydride (6.39 g, 1.5 equiv.). The reaction was then stirred under nitrogen for 1 h. After an hour, additional sodium triacetoxyborohydride (4.26 g, 1.0 equiv.) was added to the reaction and stirred further for another 1 h. The reaction mixture was then quenched with saturated $NaHCO_3$ solution (100 mL). The

 doi:10.20944/preprints202503.0093.v1

aqueous phase was extracted with CH_2Cl_2 (2 × 100 mL), and the combined organics dried over anhydrous $MgSO_4$ and concentrated to dryness *in vacuo* to afford (2-((m-tolylamino)methyl)phenyl)boronic acid **46** as a cream coloured solid (3.64 g, 75% yield). The material was used without further purification. ^{1}H NMR (400 MHz, $CDCl_3$) δ_H 7.74 (dd, *J* = 7.6, 1.5 Hz, 1H, H5), 7.45 (m, 2H, H2, H12), 7.38 – 7.32 (m, 3H, H6, H16), 7.02 – 6.97 (m, 2H, H1, H11), 6.66 (m, 2H, H10, H14), 6.52 (s, 1H, H8), 4.36 (s, 2H, H7), 2.14 (s, 3H, H15). LC-MS: retention time: 6.4 min; ESI-QTOF HRMS (m/z): for $[C_{14}H_{17}BNO_2]^+$ $[M+H]^+$: exact mass *calcd.*: 242.1352; found: 242.1354.

(E)-(2-(((3-methyl-4-((4-nitrophenyl)diazenyl)phenyl)amino)methyl)phenyl)boronic acid ***47a****:* 4-nitroaniline (504 mg, 3.64 mmol, 1.1 equiv.) was mixed in water (2 mL), methanol (2 mL) and hydrochloric acid (2 mL, 5.0 M) and then cooled to 0–5 °C on an ice-bath. A chilled solution of sodium nitrite (186 mg, 2.69 mmol, 1.3 equiv.) was added dropwise. Excess nitrite was destroyed by the addition of sulfamic acid after stirring for 5 minutes. (2-((m-tolylamino)methyl)phenyl)boronic acid (500 mg, 2.07 mmol, 1.0 equiv.) was dissolved in methanol (3 mL) and dilute hydrochloric acid (2 mL, 1 M) then added dropwise to the reaction mixture, which quickly turned red. Sodium acetate was added to raise the pH of the solution to 4 and this was then left to stir at 0–5 °C for 3 hours. Sodium hydroxide (2 M) was slowly added to raise the pH to 7. The resulting precipitate was collected by suction filtration and dried in a desiccator overnight to afford product **47a** as a dark red solid (44% yield). ^{1}H NMR (400 MHz, DMSO-d_6) δ_H 9.86 (s, 1H), 8.39 (d, *J* = 8.9 Hz, 2H), 8.33 (d, *J* = 8.9 Hz, 1H), 8.18 (s, 1H), 8.01 (d, *J* = 8.9 Hz, 2H), 7.92 – 7.85 (m, 2H), 7.75 (d, *J* = 9.1 Hz, 1H), 7.58 – 7.53 (m, 1H), 7.47 (s, 2H, 2H), 7.37 – 7.30 (m, 1H), 4.63 (s, 2H), 2.73 (s, 3H, 3H). ^{13}C NMR (101 MHz, DMSO-d_6) δ_C 156.8, 156.1, 153.6, 150.5, 148.3, 147.5, 146.5, 144.1, 142.6, 141.6, 141.5, 133.7, 130.4, 130.3, 129.0, 125.0, 123.0, 122.5, 122.4, 118.7, 116.3, 116.1, 52.7, 17.7. ^{11}B NMR (128 MHz, DMSO-d_6) δ_B 32.0. LC-MS: retention time: 9.9 min; ESI-QTOF HRMS (m/z): for $[C_{20}H_{20}BN_4O_4]^+$ $[M+H]^+$: exact mass *calcd.*: 391.1578; found: 391.1587.

(E)-4-((4-((2-boronobenzyl)amino)-2-methylphenyl)diazenyl)benzoic acid ***47b****:* The above procedure was repeated using 4-aminobenzoic acid (0.11 g, 0.83 mmol) instead of 4-nitroaniline. All other reagents were used in the same mole ratios, to afford **47b** as an orange-red solid (62% yield). ^{1}H NMR (400 MHz, DMSO-d_6) δ_H 13.09 (s, 1H), 9.79 (s, 1H), 8.15 – 8.08 (m, 2H), 8.05 (dd, *J* = 8.6, 1.9 Hz, 1H), 7.90 (dd, *J* = 8.0, 6.3 Hz, 3H), 7.79 (dd, *J* = 8.5, 1.7 Hz, 1H), 7.72 (d, *J* = 9.1 Hz, 1H), 7.68 (dd, *J* = 9.1, 2.3 Hz, 1H), 7.56 (d, *J* = 2.4 Hz, 1H), 7.48 (s, 2H), 7.35 (dd, *J* = 7.8, 4.3 Hz, 1H), 4.64 (s, 2H), 2.73 (s, 3H). ^{13}C NMR (101 MHz, DMSO-d_6) δ_C 166.9, 155.1, 149.8, 148.4, 144.0, 140.6, 131.6, 130.6, 130.5, 130.4, 130.2, 122.5, 122.2, 118.8, 116.1, 116.0, 52.7, 48.6, 30.4, 17.7. ^{11}B NMR (128 MHz, DMSO-d_6) δ_B 30.4. LC-MS: retention time: 8.2 min; ESI-QTOF HRMS (m/z): for $[C_{21}H_{21}BN_3O_4]^+$ $[M+H]^+$: exact mass *calcd.*: 390.1625; found: 390.1634. FTIR (cm^{-1}): υ(O–H st) 3442, υ(C–H st) 2925, υ(C=O st, carboxyl) 1677, υ(C=C st and C=N st) 1677–1600.

(E)-3-((4-((2-boronobenzyl)amino)-2-methylphenyl)diazenyl)benzoic acid ***47c****:* The previous experiment was repeated using 3-aminobenzoic acid (499 mg, 3.64 mmol) instead of *p*-anisidine. All other reagents were used in the same mole ratios, to afford **47c** as a red solid (25% yield). ^{1}H NMR (400 MHz, DMSO-d_6) δ_H 13.20 (s, 1H), 9.77 (s, 1H), 8.34 (t, *J* = 1.8 Hz, 1H), 8.25 – 8.16 (m, 1H), 8.10 – 8.03 (m, 3H), 7.89 (d, *J* = 7.3 Hz, 1H), 7.72 (d, *J* = 9.1 Hz, 2H), 7.70 – 7.66 (m, 2H), 7.56 (d, *J* = 2.4 Hz, 1H), 7.48 (s, 2H), 4.64 (s, 2H), 2.73 (s, 3H). LC-MS: retention time: 8.5 min; ESI-QTOF HRMS (m/z): for $[C_{21}H_{21}BN_3O_4]^+$ $[M+H]^+$: exact mass *calcd.*: 390.1625; found: 390.1630.

(E)-(2-(((4-((4-methoxyphenyl)diazenyl)-3-methylphenyl)amino)methyl)phenyl)boronic acid ***47d****:* The previous experiment was repeated using *p*-anisidine (0.61 g, 4.98 mmol, 6 equiv.) instead of 4-aminobenzoic acid. Purification was performed by washing the product (in dichloromethane) with 10% sodium hydrogen carbonate solution (w/w) to remove residual acetic acid, to yield **47d** as an orange-brown solid (56% yield). ^{1}H NMR (400 MHz, DMSO-d_6) δ_H 9.67 (s, 1H), 7.89 (d, *J* = 7.3 Hz, 1H), 7.84 (d, *J* = 8.9 Hz, 2H), 7.74 – 7.71 (m, 1H), 7.65 – 7.62 (m, 2H), 7.53 (d, *J* = 2.0 Hz, 1H), 7.48 – 7.45 (m, 2H), 7.34 (ddt, *J* = 9.2, 6.6, 3.2 Hz, 1H), 7.10 (d, *J* = 9.0 Hz, 2H), 7.08 – 7.02 (m, 1H), 4.61 (s, 2H), 3.85 (s, 3H), 2.69 (s, 3H). ^{13}C NMR (101 MHz, DMSO-d_6) δ_C 161.1, 148.4, 148.3, 146.9, 143.8, 138.9, 130.3, 130.0, 126.6, 126.4, 124.0, 123.4, 123.4, 122.5, 118.8, 115.9, 115.7, 114.5, 114.3, 55.5, 52.7, 17.7. ^{11}B NMR (128

 doi:10.20944/preprints202503.0093.v1

MHz, DMSO-d_6) δ_B 29.9. LC-MS: retention time: 9.8 min; ESI-QTOF HRMS (m/z): for $[C_{21}H_{23}BN_3O_3]^+$ $[M+H]^+$: exact mass *calcd.*: 376.1832; found: 376.1836.

2.3.8. Sudan I Dyes Boronic Acid

*Synthesis of Sudan I dyes boronic acid **48**:* To a heated solution (50 °C) of Sudan I (347 mg, 1.39 mmol, 1.2 equiv.) in acetone (20 mL), potassium carbonate, K_2CO_3 (128 mg, 0.93 mmol, 0.80 equiv.) and 4-(bromomethyl)phenylboronic acid (250 mg, 1.16 mmol, 1.0 equiv.) were added. After 4 h of stirring and heating, additional potassium carbonate, K_2CO_3 (128 mg, 0.93 mmol, 0.80 equiv.) was added, and the suspension was stirred overnight. Finally, the reaction mixture was diluted with EtOAc and the organic layer was washed with 1 M hydrochloric acid (2 × 10 mL) and brine (20 mL), dried over Na_2SO_4, and concentrated *in vacuo*. The resulting solid was further purified using silica gel chromatography affording a pure Sudan I dye boronic acid **48** product. LC-MS: retention time: 9.7 min; ESI-QTOF HRMS (m/z): for $[C_{23}H_{19}BN_2O_3]^+$ $[M+H]^+$: exact mass *calcd.*: 383.2260; found: 383.1572.

2.4. Measurements of Photophysical Properties of Synthesized Compounds

Photophysical quantities such as absorption maxima (λ_{abs}^{max}), emission maxima (λ_{em}^{max}), Stokes shift ($\Delta\lambda$), molar extinction coefficient (ε), fluorescence quantum yield (Φ_F), and brightness were determined from absorption and emission data. Photophysical measurements were done at ambient temperature (25 °C). UV-vis absorption spectra were recorded on a Shimadzu UV-1800 spectrophotometer between 200 and 800 nm using quartz cuvettes of 1 cm optical path length. The molar extinction coefficients (ε) of the different arylboronic acid dyes were determined at the respective maximum absorption wavelength using the Beer-Lambert law:

$$A = \varepsilon cl \quad (1)$$

Where: A is absorbance; ε the extinction coefficient for the dye; c is the sample concentration; l is the pathlength of the sample cuvette. Fluorescence spectra of the synthesized compounds were acquired using a Shimadzu RF-6000 spectrofluorometer (Shimadzu, Kyoto, Japan). Emission spectra were recorded at room temperature with excitation wavelengths set at the λ_{abs}^{max} of the respective dyes and emission range 250–800 nm. The excitation and emission slit widths were set at 5 nm. Fluorescence quantum yields were determined by the relative comparison procedure [64,65], using either rhodamine B (Φ_F = 0.70 in ethanol)[66] or quinine sulfate (Φ_F = 0.51 in 0.05 M H_2SO_4) [4,67]. Five different solutions with increasing concentrations of each of the synthesized compounds and the reference standards (rhodamine B or quinine sulfate) were prepared in different solutions and the absorbance of each solution was determined to be between 0.01 – 0.1 in 1 cm optical path length cuvette using a Shimadzu UV-1800 Spectrophotometer. Fluorescence spectra and the integrated fluorescence intensities for varying concentrations of solutions were measured using a Shimadzu RF-6000 spectrofluorometer. For each solution, graphs of the integrated fluorescence intensities as a function of the solution absorption were plotted in each case for both the synthesized dye and the reference standard (either rhodamine B or quinine sulfate). The resulting data points were fitted with linear plots and the slopes were calculated. The quantum yield (Φ_F) is calculated using the slope of the line determined from the plot of the absorbance against the integrated fluorescence intensities. In this case, the quantum yield of the unknown sample can be calculated using the equation:

$$\Phi_{F,S} = \Phi_{F,R}\left(\frac{m_S}{m_R}\right)\left(\frac{\eta_S^2}{\eta_R^2}\right) \quad (2)$$

Where: m is the slope of the line obtained from the plot of the integrated fluorescence intensity vs. absorbance, η is the refractive index of solvent and the subscripts R and S refer to the reference and unknown sample respectively; Φ_S and Φ_R are the fluorescence quantum yield of the sample and that of the standard respectively. The quantum yields were corrected for the differing refractive index of the solvent used for the sample and reference. Refractive indices (25 °C) were taken to be 1.3326,

 doi:10.20944/preprints202503.0093.v1

1.3593, and 1.4793 for water, ethanol, and DMSO respectively [68]. In instances where the same solvent was used for both reference and unknown sample as a solvent, $\left(\eta_S^2/\eta_R^2\right)$ will be 1, so the fluorescence quantum yield of the unknown (Φ_S) was obtained directly from the quotient of the two slopes.

3. Results and Discussion

3.1. Synthesis of Various Arylboronic Acid Chemosensors Fluorescent Dyes

3.1.1. Synthesis of the Building Blocks Through Miyaura Borylation

The syntheses of the various boronic ester building blocks were accomplished *via* a palladium-catalyzed Miyaura borylation of aryl halides with a diboron reagent such as bis(pinacolato)diboron (B_2pin_2). Potassium acetate (KOAc) was employed as the base, and the reaction was carried out in 1,4-dioxane at 80 °C for 16 h [69–71]. The various pinacol-protected boronate esters were readily purified by silica gel chromatography to obtain analytically pure and white crystalline pinacol boronate ester solids with yields ranging from 70% to 96% (Scheme 1). They were characterized by ^{1}H and ^{13}C NMR, FTIR and HRMS and the data are provided in the Materials and Methods section with the corresponding spectra available in the Electronic Supplementary Information (Figures S1–S5). Interestingly, these boronate ester solids are indefinitely bench-stable under air compared to their corresponding boronic acids.

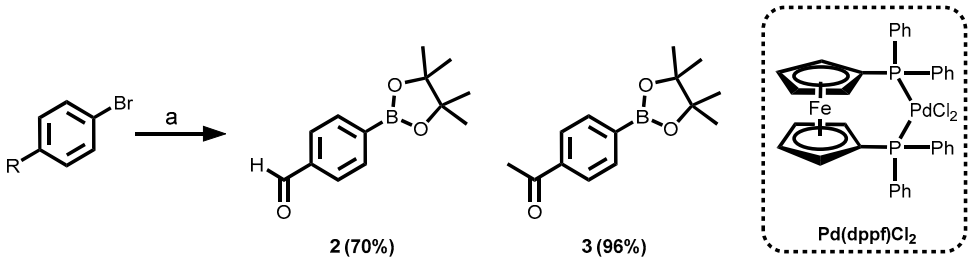

Scheme 1. Palladium-catalyzed Miyaura borylation of aryl halides utilizing bis(pinacolato)diboron. Reagents and conditions: (a) bis(pinacolato)diboron, KOAc, $Pd(dppf)Cl_2$, 1,4-dioxane, 80 °C, 16 h.

3.1.2. Coumarin-Tagged Boronic Acids

Coumarin and its derivatives are widely used as fluorescent probes because of their excellent chromogenic and fluorogenic properties such as high fluorescence quantum yields, large Stokes shifts, excellent photostability, and thermal stability [72–78]. Based on this knowledge, two coumarin-tagged boronic acids were designed and synthesized (Schemes 2 and 4). The synthesis of the target compound **7** was achieved in four chemical steps as shown in Scheme 2. Characterization was done by ^{1}H and ^{13}C NMR, FTIR and HRMS and the data are provided in the Materials and Methods section, and the corresponding spectra are available in the Electronic Supplementary Information (Figures S6–S18). The first step of the synthesis was *via* Knoevenagel condensation reaction of 4-(diethylamino)-2-hydroxybenzaldehyde with diethyl malonate in the presence of piperidine, cyclized and then decarboxylated to afford 7-(diethylamino)-2*H*-chromen-2-one **4** in good yield (85%). Subsequently, compound **4** was subjected to Vilsmeier–Haack formylation in the presence of 1,2-dichloroethane (DCE) to produce 7-(diethylamino)coumarin-3-carbaldehyde **5** in 79% [78].

 doi:10.20944/preprints202503.0093.v1

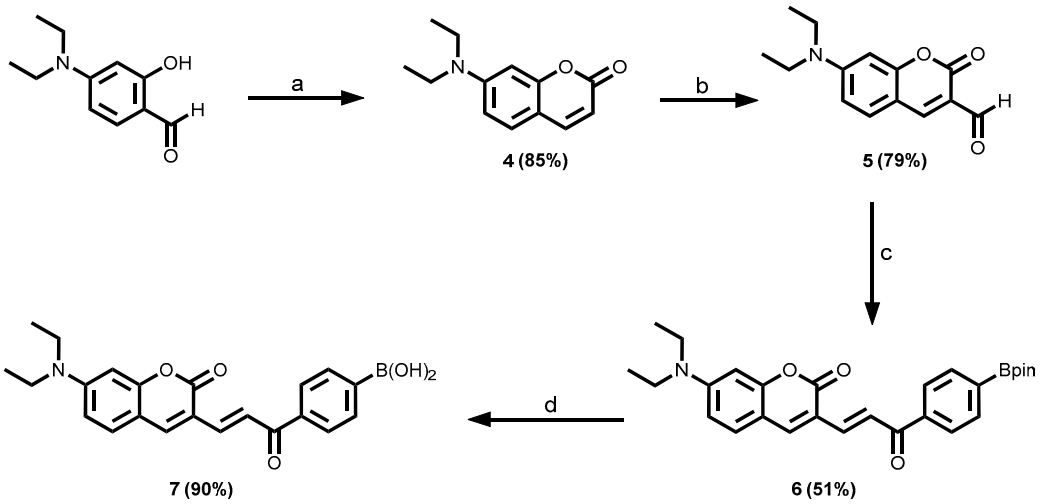

Scheme 2. Synthesis routes of coumarin-tagged boronic acid **7**. Reagents and conditions: (a) diethyl malonate, piperidine, EtOH, reflux, 13 h (**4**, 85%); (b) DMF/$POCl_3$, 1,2-dichloroethane, 0 °C → 60 °C, 12 h (**5**, 79%); (c) **3**, CH_2Cl_2/anhydrous CH_3CH_2OH=1:1 (*v*/*v*)), pyrroline, room temperature, 4 d (**6**, 51%); (d) $NaIO_4$, THF/H_2O (4:1), room temperature, 30 min (**7**, 90%).

The formylation was deemed successful by the confirmation of the distinctive and unmistakable singlet at δ_H = 10.10 ppm observed in the ^1H NMR spectrum which integrated for a single proton. This is characteristic of aldehydic protons [79].

Next, a base-catalyzed Claisen–Schmidt condensation of 7-(diethylamino)coumarin-3-carbaldehyde **5** with 1-(4-(4,4,5,5-tetramethyl-1,3,2-dioxaborolan-2-yl)phenyl)ethan-1-one **3** building block using a catalytic amount of pyrrolidine in CH_2Cl_2/EtOH afforded the chalcone molecule **6** (yield = 51%) with extended conjugations [80]. Afterwards, the chalcone **6** which had the pinacol-protecting group was subjected to an oxidative hydrolysis deprotection protocol with aqueous sodium periodate ($NaIO_4$). This led to the smooth formation of the corresponding boronic acid **7** with excellent yield (up to 90%) [8,81]. ^1H NMR analysis of the product showed that the desired final compound was prepared following the disappearance of the Bpin peak at δ_H = 1.32 ppm (see Supplementary Materials Figure S14).

Another coumarin fluorescent dye arylboronic acid was synthesised from 7-hydroxycoumarin (umbelliferone). Unbelliferone is a known fluorophore with a high quantum yield [82,83]. The coumarin-tagged boronic acid derivative in Scheme 3 was synthesised according to the procedure reported by Palanisamy *et al*. *via* a one-step alkylation reaction of 4-methylumbelliferone with 4-bromomethylphenylboronic acid in the presence of anhydrous potassium carbonate in dry DMF at 70 °C [84] to afford **22** in 76% yield after purification. The product was fully characterised by ^1H and ^{13}C NMR, and HRMS data as provided in the Materials and Methods section and the corresponding spectra are available in the Electronic Supplementary Information (Figures S19–S23).

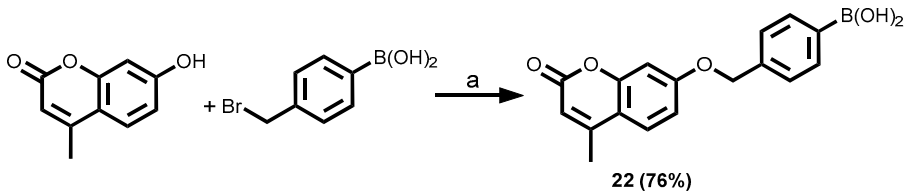

Scheme 3. Synthetic route to arylboronic acid dye 22. Reagents and conditions: (a) Cs_2CO_3, DMF, 70 °C, reflux, 1.5 h (22, 76%).

Preprints.org (www.preprints.org) | NOT PEER-REVIEWED | Posted: 4 March 2025 doi:10.20944/preprints202503.0093.v1

3.1.3. 9-Aminoacridine-Tagged Boronic Acid Dyes

In another development, 9-aminoacridine-tagged boronic acid dyes were prepared. 9-Aminoacridine is a quinoline derivative that contains a tacrine-like moiety (Figure 4). Acridine and its derivatives are important quinoline structural derivatives that are generally planar tricyclic aromatic molecules which fluoresce at shorter wavelength regions [85,86]. Acridine-based fluorescence chemosensors have recently been synthesized and employed by Wang *et al*. for the selective detection of Fe^{3+} and Ni^{2+} ions [87].

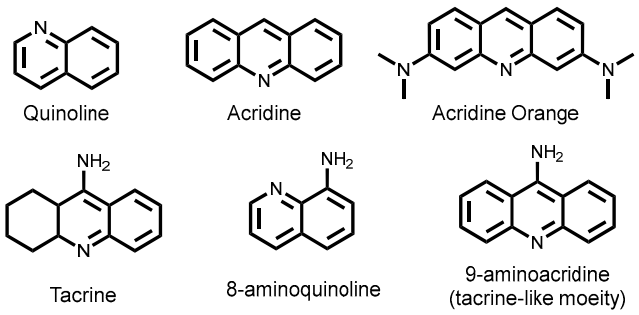

Figure 4. Structures of quinoline and quinoline derivatives.

Harnessing the advantages of the acridine moiety, a new arylboronic acid fluorescent chemosensor was prepared by coupling an aminoacridine fluorophore to a (4-(aminomethyl)phenyl)boronic acid *via* a chloroacetyl chloride linker in three steps (Scheme 4). *N*-(acridin-9-yl)-2-chloroacetamide **23** was prepared by reacting a commercially available 9-aminoacridine with chloroacetyl chloride according to chloroacetylation reaction procedures described in the literature [88–90]. This step was carried out in the presence of a catalytic amount of triethylamine (Et_3N). Chloroacetyl chloride plays a key role in synthetic and biological chemistry as a bifunctional linker for alcohols and amines [91]. Thus, it was employed to prepare the *N*-(acridin-9-yl)-2-chloroacetamide **23** as a suitable building block for the next step. The reaction was run overnight under room temperature, and the isolated yield was 59%. (4-(Aminomethyl)phenyl)boronic acid was then alkylated with the *N*-(9-acridinyl)-2-chloroacetamide using triethylamine as a catalyst under reflux in acetonitrile (CH_3CN) for 24 h to provide the target compound (4-(((2-(acridin-9-ylamino)-2-oxoethyl)amino)methyl)phenyl)boronic acid **24** in 22% yield.

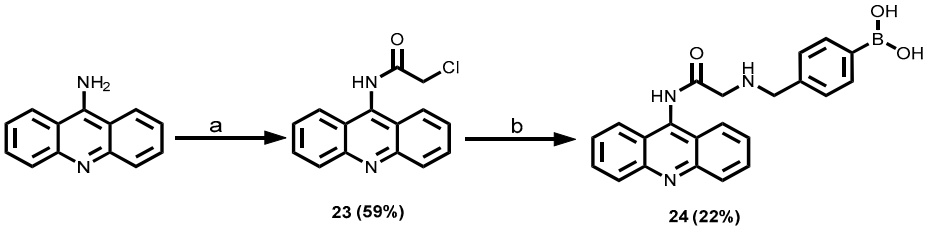

Scheme 4. Synthetic route to (4-(((2-(acridin-9-ylamino)-2-oxoethyl)amino)methyl)phenyl)boronic acid **24**. Reagents and conditions: (a) chloroacetyl chloride, Et_3N, THF, 0 °C to room temperature, overnight (**23**, 59%); (b) (4-(aminomethyl)phenyl)boronic acid, Et_3N, CH_3CN, reflux, 24 h (**24**, 22%).

3.1.4. 8-Aminoquinoline-Tagged Boronic Acid Dyes

8-aminoquinoline contains a quinoline moiety which is a well-known fluorophore unit [92]. Quinolines are particularly desirable because of their good coordination properties and their ability to form hydrogen bonds as a result of the presence of nitrogen in the ring as well as its small molecular size [92,93]. Furthermore, they are well known for their good metal affinity and hence are becoming

 doi:10.20944/preprints202503.0093.v1

leading candidates in the design of fluorescent probes for metals such as zinc and their applications in more complex biological research [92]. More importantly, the chemistry of quinoline is also well established and a plethora of synthetic methods available to functionalize the core moiety [92]. With these advantages, attempts were made to synthesize an aminoquinoline-tagged boronic acid **29**. The synthesis was achieved in five steps as depicted in Scheme 5. The first step involves *Boc*-protection of glycine by reacting with *di-tert*-butyl dicarbonate (Boc_2O) under basic conditions to afford *Boc*-Gly-OH under 2 hours. This was followed by amide coupling between the carboxylic acid functionality of the *N-Boc* protected glycine **25** and 8-aminoquinoline in CH_2Cl_2 in the presence of EDC.HCl/DMAP as the activation/amide coupling agent.

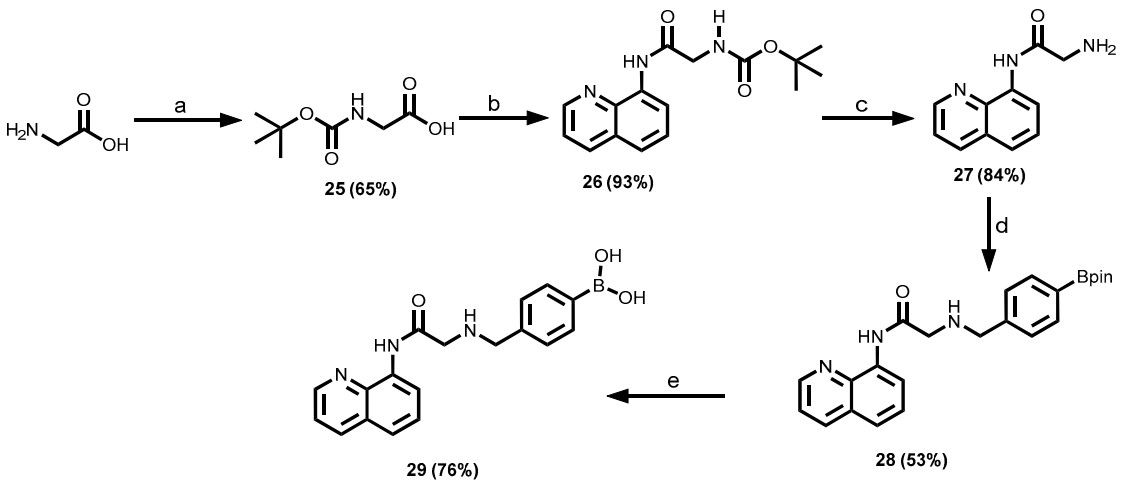

Scheme 5. Synthetic route to (4-(((2-oxo-2-(quinolin-8-ylamino)ethyl)amino)methyl)phenyl)boronic acid **18.** Reagents and conditions: (a) $(Boc)_2O$, Et_3N, 1,4-dioxane/H2O (1:1), room temperature, 2 h (**6**, 65%); (b) 8-aminoquinoline, EDC.HCl, DMAP, CH_2Cl_2, room temperature, overnight (**15**, 93%); (c) HCl/dioxane (6 N), CH_2Cl_2, room temperature, overnight (**16**, 84%); (d) **2**, $NaBH(OAc)_3$, 1,2-dichloroethane, room temperature, 2 h (**28**, 53%); (e) $NaIO_4$, THF/H_2O (4:1), room temperature, 30 min (**29**, 76%).

The next step was to obtain the free amine through deprotection of the *N-Boc* group by using the traditional approach based on TFA-induced cleavage as reported previously [94] or with HCl (6 M) in dioxane at room temperature [95,96]. Both methods gave the desired products in excellent yields. The resultant free base was characterised by NMR and used in the next step without further purification. After the successful deprotection of the *N-Boc* group to obtain the free amine **27**, it was then coupled to the aldehyde functionality of the pinacol-protected 4-formylphenylboronic acid **2** building block that was previously synthesized under reductive amination conditions to give the aminomethyl derivative **28.** Sodium triacetoxyborohydride ($NaBH(OAc)_3$) was chosen as the reducing agent over others such as sodium cyanoborohydride ($NaBH_3CN$) and the less bulky hydride reagents, $NaBH_4$ because of its high efficiency in reductive amination reactions with unreactive amines leading to faster, better yields, and with fewer side products. Secondly, $NaBH(OAc)_3$ has been reported to be more selective for direct reductive aminations of ketones and aldehydes relative to the sodium cyanoborohydride alternative [97]. The other advantage of triacetoxyborohydride is the avoidance of the production of toxic by-products such as NaCN and HCN that are usually associated with the use of $NaBH_3CN$ [28]. 1,2-dichloroethane (DCE) was preferred as reaction solvent even though other similar amination reactions have been carried out in other solvents such as tetrahydrofuran (THF) and acetonitrile (CH_3CN). The final step was the deprotection of the boronate ester **28** using the optimized procedure of $NaIO_4$ to afford (4-(((2-oxo-2-(quinolin-8-ylamino)ethyl)amino)methyl)phenyl)boronic acid **29** in 76% yield.

Preprints.org (www.preprints.org) | NOT PEER-REVIEWED | Posted: 4 March 2025 doi:10.20944/preprints202503.0093.v1

3.1.5. Fluorescein-Tagged Boronic Acid Dyes

The synthesis of fluorescein-tagged boronic acid **36** was performed following the procedure in Scheme 6. First, esterification of cyclic fluorescein was carried out in the presence of a catalytic amount of concentrated sulfuric acid in methanol to afford fluorescein methyl ester **34** in an excellent yield (93%). The fluorescein methyl ester intermediate **34** was first characterized by X-ray crystallography (**the crystallographic data is shown in** Table S1). Full crystallographic data are available in the Cambridge crystallographic data centre with CCDC number: 2426549. This data can be obtained free of charge via https://www.ccdc.cam.ac.uk/ structures/ from the Cambridge Crystallographic Data Centre. Then the ester was refluxed for 6 h with an excess amount of hydrazine hydrate in methanol *via* hydrazinolysis to produce the desired fluorescein hydrazide **35** with a yield of 96% yield [98]. An alternative method for the preparation of fluorescein hydrazide **35** (in 89% yield) involved the direct hydrazinolysis of the cyclic fluorescein using excess hydrazine hydrate under reflux in methanol for 12 h. Finally, through Schiff base reaction, the fluorescein hydrazide **35** was coupled to 4-formylphenylboronic acid to form the fluorescein-tagged arylboronic acid chemosensor **36** in 64% yield.

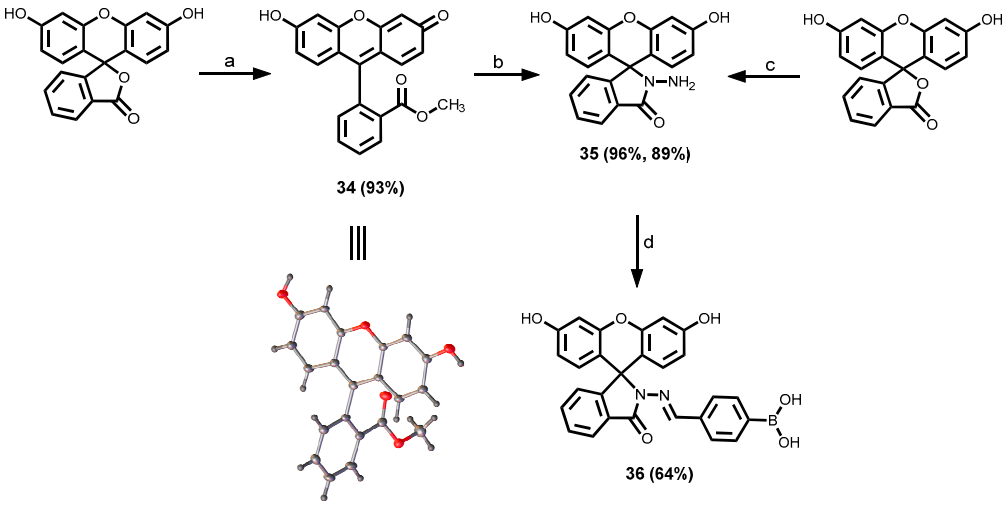

Scheme 6. Synthetic route to *(E)*-(4-(((3',6'-dihydroxy-3-oxospiro[isoindoline-1,9'-xanthen]-2-yl)imino)methyl)phenyl)boronic acid. Reagents and conditions: (a) MeOH/H_2SO_4, reflux, 6 h (**34**, 93%); (b) $NH_2NH_2 \bullet H_2O$/MeOH, reflux, 6 h (**35**, 96%); (c) $NH_2NH_2 \bullet H_2O$/MeOH, reflux, 12 h (**35**, 89%); (d) 4-formylphenylboronic acid, EtOH, reflux, 5 h (**36**, 64%).

A second fluorescein boronic acid was synthesized *via* a one-step reaction of fluorescein isothiocyanate isomer I and 3-aminobenzeneboronic acid (Scheme 7). The fluorescein isothiocyanate contains an electrophilic carbon atom that readily reacted with nucleophile (amine) using dimethylformamide (DMF) as the solvent to form thiourea compound **37** in 68% yield [99,100].

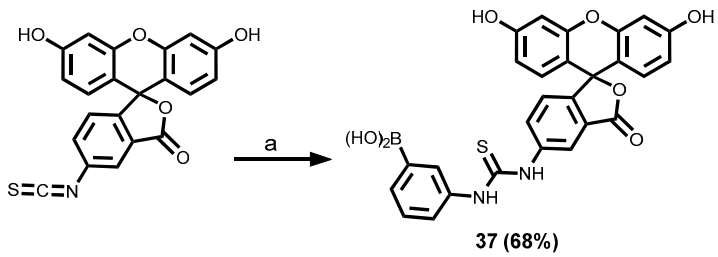

Scheme 7. Synthesis of (3-(3-(3',6'-dihydroxy-3-oxo-3H-spiro[isobenzofuran-1,9'-xanthen]-5-yl)thioureido)phenyl)boronic acid. Reagents and conditions: (a) 3-aminobenzeneboronic acid, DMF, room temperature, 12 h (**37**, 68%).

 doi:10.20944/preprints202503.0093.v1

3.1.6. Rhodamine-Tagged Boronic Acid Dye

Rhodamine dye fluorophores are part of the family of xanthenes along with fluorescein and eosin dyes [101]. The structures of xanthene chromophore and rhodamine dyes are shown in Figure 5. The carboxylic acid group of rhodamine dyes undergo intramolecular cyclization. The ring-opened form is highly fluorescent, whereas the spirocyclic spirolactone form is essentially nonfluorescent [101–103].

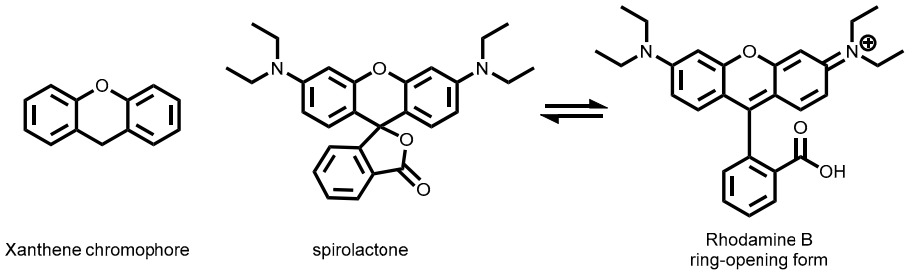

Figure 5. Molecular structure of Xanthene and Rhodamine B dye.

Rhodamine dyes and their derivatives have also been used extensively, in particular, as chemosensors either *in vitro* or *in vivo* in the detection of metals including Hg(II) [104–106], peroxynitrite [52], Cu(II) [107], Fe(III) [108], Cr(III) [108]. Rhodamine derivatives are also employed as molecular switches [109]. Rhodamine B was chosen as the fluorescent dye for use in this study due to the high fluorescence quantum efficiency, high molar extinction coefficients, and low cost. A rhodamine-tagged boronic acid **39** was readily synthesized from rhodamine B by a two-step reaction (Scheme 8), where rhodamine B was treated with excess hydrazine in methanol to give rhodamine B hydrazide **38** in 68% yield. The hydrazide was further converted to the designed product **39** in 73% yield through a Schiff base reaction using 4-formylphenylboronic acid.

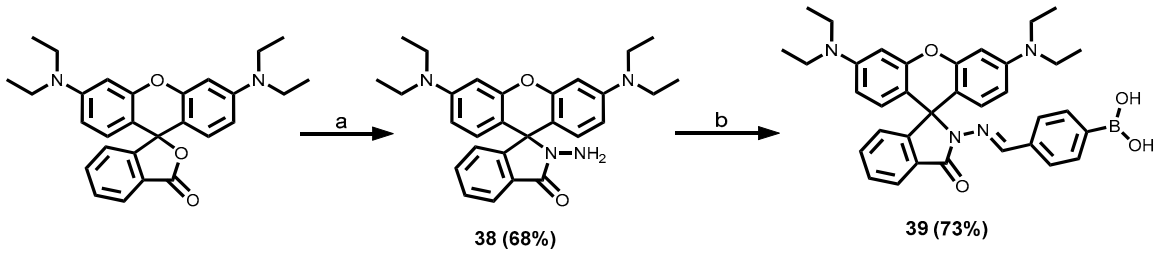

Scheme 8. Synthesis of (E)-(4-(((3',6'-bis(diethylamino)-3-oxospiro[isoindoline-1,9'-xanthen]-2-yl)imino)methyl)phenyl)boronic acid **39**. Reagents and conditions: (a) $NH_2NH_2 \bullet H_2O$/MeOH, reflux, 6 h (**38**, 68%); (b) 4-formylphenylboronic acid, EtOH, reflux, 5 h (**39**, 73%).

3.1.7. BODIPY-Tagged Boronic Acid Dyes

4,4-difluoro-4-bora-3a-4a-diaza-s-indacene (simply known as BODIPY, difluoroboron dipyrromethene) and its derivatives are fluorescent organic dye molecules that were first discovered by Treibs and Kreuzer in 1968 [110] (Figure 6). Since then, several BODIPY and their derivatives have become the most popular dye molecules among the multitude of fluorescent dyes available with widespread applications in various areas including tunable laser dyes, biological labelling [111–113], as fluorescent switches, fluorophores in sensors and labels, and light-harvesting systems in electroluminescent devices [114–116]. The interest in BODIPY chromophores can be attributed to their favourable physicochemical characteristics and desirable photophysical properties [117,118], such as high fluorescence quantum yields, relatively large molar absorption coefficient, narrow emission bandwidths, and tunable fluorescent properties as well as relatively high thermal and photochemical stabilities [119–122]. These molecules generally have excitation/emission wavelength

 doi:10.20944/preprints202503.0093.v1

in the visible region with stable excited states. Other advantages include ease of modification of BODIPY chemically for the synthetic accessibility of various derivatives and good solubility in common solvents [123]. As a result, a significant number of BODIPY derivatives have since been synthesized and characterized [119,120]. Also, there is an abundance of literature that supports the synthetic versatility of the BODIPY chromophore which allows for far-reaching structural modifications resulting in the alteration of the electronic, optical and chemical properties of the dye [124].

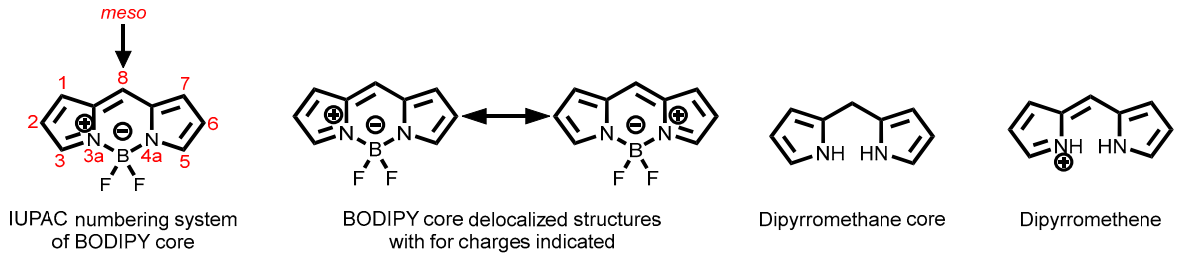

Figure 6. Representation of the BODIPY framework showing the IUPAC numbering system, delocalized structures, dipyrromethene and dipyrromethene cores.

Thus, a procedure for the introduction of an arylboronic acid unit onto a BODIPY core was developed to take advantage of the desirable photophysical properties outlined above. Two approaches were employed to synthesise the boron dipyrromethene (BODIPY)-tagged boronic acid dye **45** (Scheme 9). The first route involved the use of the pinacol-protected 4-formylphenylboronic acid **2,** whereas in the second route, 4-formylphenylboronic acid was attempted directly without protecting it to reduce the number of steps especially in instances where purification and hydrolysis of the boronate proved challenging. The synthesis began with an acid-catalyzed condensation between two equivalents of 2,4-dimethylpyrrole and a suitable electrophile such as pinacol-protected 4-formylphenylboronic acid **2** to form a dipyrromethane intermediate **40** followed by the addition of a few drops of trifluoroacetic acid (TFA). The complete consumption of the aldehyde was monitored by TLC. The dipyrromethane intermediate **40** was unstable and was therefore not isolated but converted directly to a dipyrromethene **41** in an oxidation step carried out using 2,3,5,6-tetrachloro-p-benzoquinone (*p*-chloranil) as an oxidant [125]. The dipyrromethene **41** was subsequently subjected to a boron trifluoride etherate ($BF_3{\cdot}Et_2O$) complexation reaction catalyzed by triethylamine (Et_3N) to afford the borondifluoride complex **42** in 47% yield [126,127]. The last step involved the deprotection of the boronate ester **42,** in the case where the protected boronate aldehyde was used, to obtain the BODIPY dye **45** as a red crystalline solid (89% yield).

A single-crystal diffraction analysis was measured for crystals of **45,** and the Oak Ridge thermal ellipsoid plot (ORTEP) diagram is displayed in Figure 7 and the crystallographic data is shown in Supplementary Materials (Table S1.). The crystal structure of BODIPY **45** reveals that the molecule is virtually planar. This is corroborated by the following structure refinement data. The boron atom has a slightly distorted tetrahedral coordination with the two fluorine atoms being perpendicularly oriented with respect to the dipyrrin plane. The B1–N1 and B1–N2 bond lengths are 1.536(2) Å and 1.534(2) Å respectively. Likewise, the B1–F1 and B1–F2 bond lengths are 1.412(2) Å and 1.407(2) Å respectively. The bond distances of the two B–N and two B–F are virtually identical which is an indication that **45** possess single B–N and B–F bonds. Also, the average N1–B1–N2 and F1–B1–F2 angles are 107.75(12) ° and 106.82(12)°, respectively. This also presupposes that there is an expected delocalisation of the positive charge. Also, full crystallographic data are available in the Cambridge crystallographic data centre with CCDC number: 2426501. This data can be obtained free of charge via https://www.ccdc.cam.ac.uk/ structures/ from the Cambridge Crystallographic Data Centre.

Preprints.org (www.preprints.org) | NOT PEER-REVIEWED | Posted: 4 March 2025 doi:10.20944/preprints202503.0093.v1

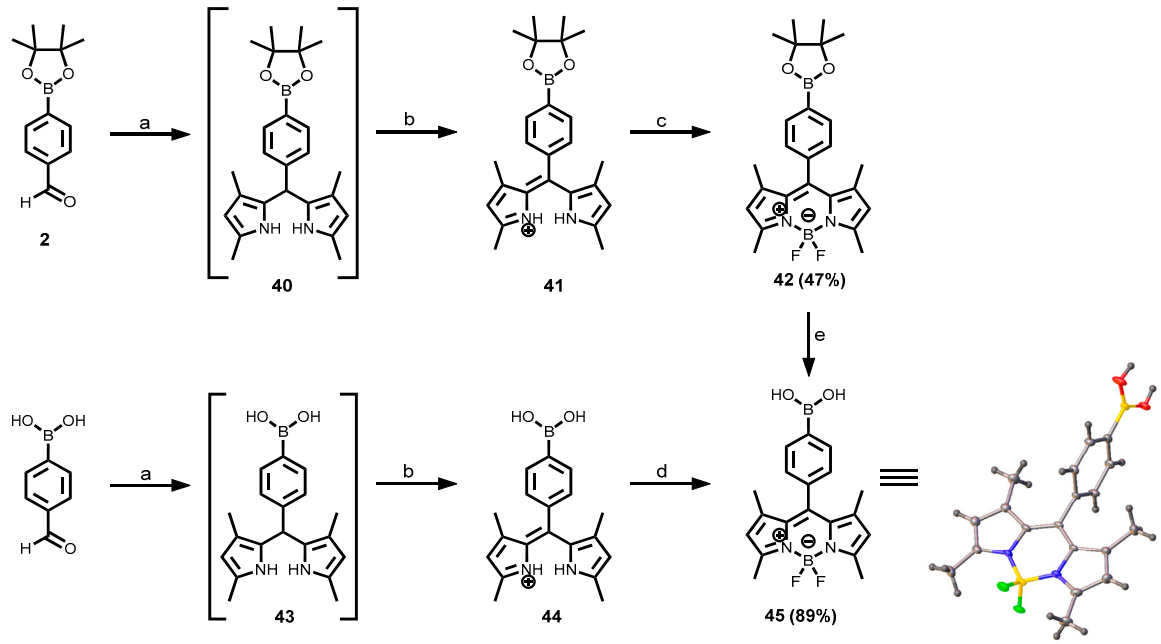

Scheme 9. Synthesis of BODIPY-tagged boronic acid **45** *via* two routes. Reagents and conditions: (a) 2,4-dimethylpyrrole, CH_2Cl_2, 0 °C to room temperature, 3 h; (b) *p*-chloranil, CH_2Cl_2, 0 °C to room temperature, 30 min; (c) Et_3N, BF_3•OEt_2, CH_2Cl_2, 0 °C to room temperature, 12 h (**42,** 47%); (d) Et_3N, BF_3•OEt_2, CH_2Cl_2, 0 °C to room temperature, 12 h (**45,** 89%); (e) $NaIO_4$, THF/H_2O (4:1), room temperature, 30 min (**45**, 89%).

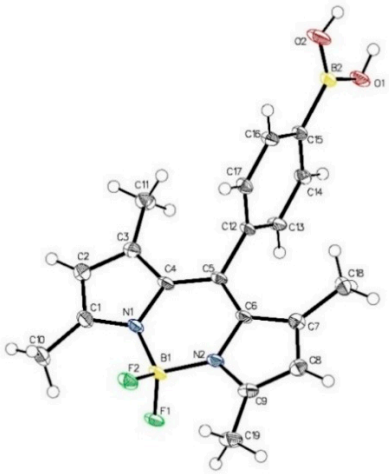

Figure 7. ORTEP representation of the compound **45** investigated by X-ray structure analysis; atomic labelling shown with 30% probability displacement ellipsoids.

3.1.8. Azo-Tagged Boronic Acid Dyes

Boronic acid azo dyes were used in the 1940s for investigations in the treatment of cancer by boron neutron capture therapy (BNCT) [128]. However, in 1991, a boronic acid azo dye synthesized from 4-aminophenylboronic acid was found to be sensitive to a selection of saccharides [129]. Subsequently, various conjugates of azo dyes have been developed as saccharide and sugar sensors [130–132]. A variety of azo-tagged boronic acid dyes in which subtle modifications are made to the electronic configuration of the azo chromophore by varying the substituent groups on the azo aromatic ring were synthesised as depicted in Scheme 10. The first step involved the synthesis of (2-((m-tolylamino)methyl)phenyl)boronic acid **46** by reductive amination followed by diazotization of various anilines containing electron-withdrawing groups such as *p*-NO_2, *p*-COOH, *p*-OCH_3, and *m*-COOH in the presence of an aqueous solution of sodium nitrite ($NaNO_2$) in concentrated HCl

 doi:10.20944/preprints202503.0093.v1

medium at 0 °C to form the corresponding diazonium salts. The destruction of excess sodium nitrite after the diazotization reaction step was required because nitrites are toxic and can be harmful to the environment. This was achieved by using a common nitrous acid scavenger such as sulfamic acid (H_3NSO_3) that reacts with nitrous acid (HNO_2) to form stable and non-toxic compounds [133,134]. The diazonium salts that were formed in the previous step were not isolated but coupled *in situ* with (2-((*m*-tolylamino)methyl)phenyl)boronic acid **46** in a basic medium (NaOH) to give the respective target products which were fully characterized by ^{1}H NMR, ^{13}C NMR and HR-LCMS spectroscopic and spectrometric analysis. It is worth noting that the pH of the reaction mixture plays a significant role in the coupling reaction and therefore a careful balance must be struck between the equilibria governing the coupling component and the diazo component. The coupling reactions of the various aniline diazonium salts with the (2-((m-tolylamino)methyl)phenyl)boronic acid **46** occur predominantly para to the electron-donating anilinic nitrogen because of steric effects. This was directed by incorporating a methyl group *meta* to the anilinic nitrogen in the amine coupling agent, and it resulted in the exclusive para coupling products. This approach allowed for the synthesis of target compounds (**47a – d**) and that avoided potentially difficult separation of isomers [135].

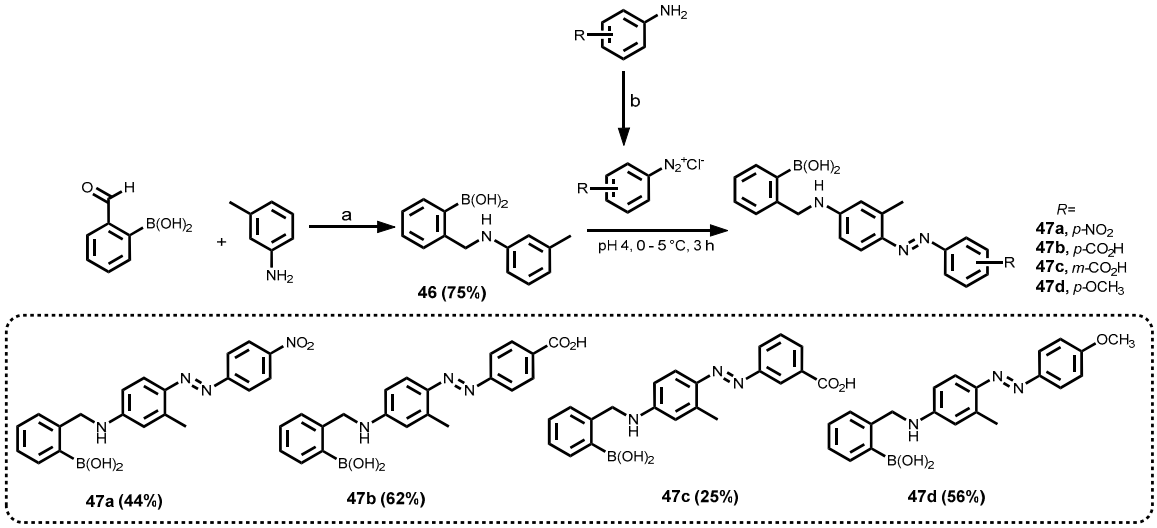

Scheme 10. Synthetic route to (E)-(2-(((3-methyl-4-(phenyldiazenyl)phenyl)amino)methyl)phenyl)boronic acid derivatives. Reagents and conditions: (a) $NaBH(OAc)_3$, 1,2-dichloroethane, room temperature, 2 h (**46**, 75%); (b) $NaNO_2$/conc HCl, 0 °C to 5 °C; (c) pH 4, 0 °C to 5 °C, 3 h.

3.1.9. Sudan I Boronic Acid Dye

Another azo boronic acid derivative was synthesised from Sudan I dye according to the one-step procedure in Scheme 11. Sudan I was reacted with 4-bromomethylphenylboronic acid in the presence of anhydrous potassium carbonate in dry acetone at 50 °C to afford **48**. The product was characterised by HRMS.

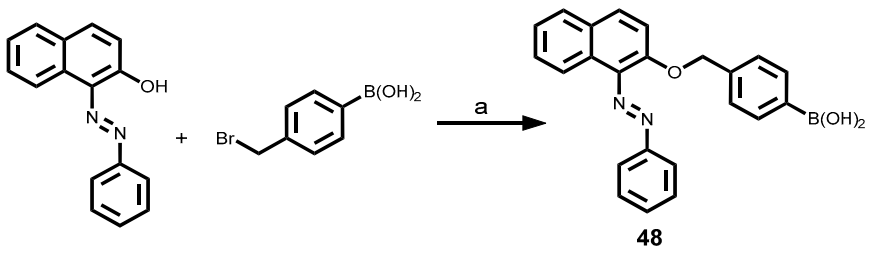

Scheme 11. Preparation of Sudan I boronic acid dye **48**. Reagents and conditions: (a) K_2CO_3, acetone, reflux, 50 °C, overnight.

Preprints.org (www.preprints.org) | NOT PEER-REVIEWED | Posted: 4 March 2025 doi:10.20944/preprints202503.0093.v1

3.2. Photophysical Properties of the Different Arylboronic Acid Chemosensor Dyes

A complete set of basic photophysical quantities such as absorption maxima (λ_{abs}^{max}), emission maxima (λ_{em}^{max}), Stokes shift ($\Delta\lambda$), molar extinction coefficient (ε), fluorescence quantum yield (Φ_F), and brightness of twelve (12) synthesized arylboronic acid chemosensors and two (2) commercially available boronic acids (2-naphthylboronic acid (BA) and 9,9-diphenyl-9H-fluoren-4-ylboronic acid (BA18) were determined in different solvents including ethanol, dimethyl sulfoxide, and methanol through absorption and emission spectroscopy techniques. The data are summarized in Figure 8 and Table 1.

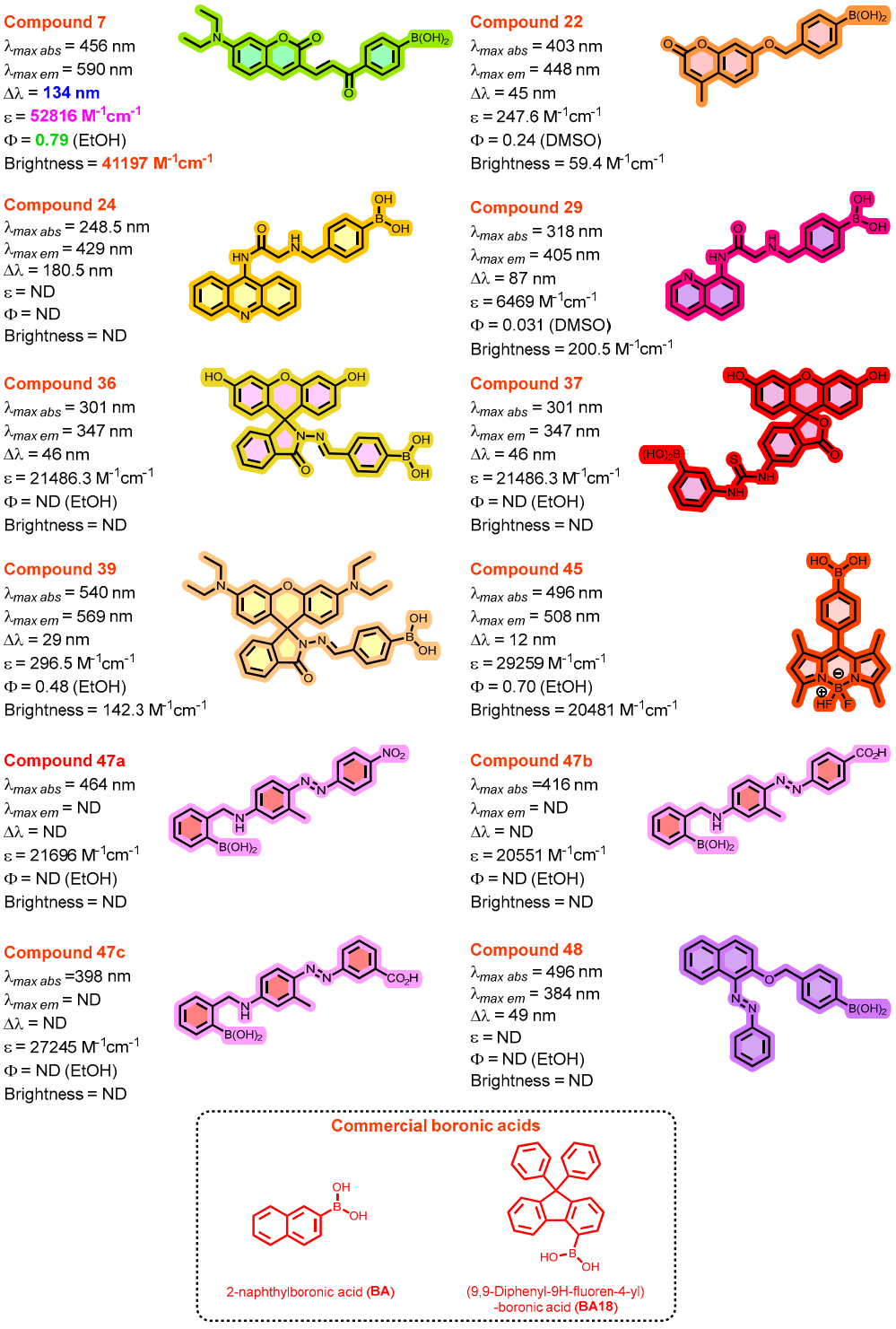

Figure 8. Structures of synthesized fluorescent arylboronic acid dyes were included in this study. The characteristic chromophore cores of the structures are highlighted in different colours.

 doi:10.20944/preprints202503.0093.v1

The UV-vis absorption spectra of the different synthesized compounds are depicted in Figure 8(see also the Supplementary Materials). The absorption maxima wavelengths are recorded in Table 1. The UV–vis spectroscopy was also used to obtain the experimental extinction coefficient (ε). It was observed that the synthesized compounds were characterized by ε ranging from very low values for **22** (ε = 248 ±16 $M^{-1}cm^{-1}$ at 403 nm) to the largest for **7** (ε = 52816 ± 1481 $M^{-1}cm^{-1}$ at 456 nm).

Table 1. Photophysical properties of synthesized fluorescent arylboronic acid dyes.

Dye	MW [gmol^{-1}]	Solvent	λ_{abs}^{max} [nm]	λ_{em}^{max} [nm]	Stokes Shift (Δλ) [nm]	ε [$M^{-1}cm^{-1}$]	Quantum yield (Φ_F)	Brightness [$M^{-1}cm^{-1}$]
7	391.2	EtOH	456	590	134	52816.1	0.78	41196.6
22	310.1	DMSO	403	448	45	247.6	0.24	59.4
24	385.2	MeOH	248.5	429	180.5	ND		ND
29	335.2	DMSO	318	405	87	6468.8	0.031	200.5
36	478.3	EtOH	301	347	46	21486.3		ND
37	526.3	EtOH	480	525	45	9368.7	0.47	4403.3
39	588.5	EtOH	540	569	29	296.5	0.48	142.3
45	368.0	EtOH	496	508	12	29259.1	0.70	20481.4
47a	390.2	EtOH	464	-	-	21695.7		ND
47b	389.2	EtOH	416	-	-	20550.8		ND
47c	389.2	EtOH	398	-	-	27245.4		ND
48	382.2	MeOH	335	384	49	ND		ND
BA	172.0	MeOH	275	328	53	ND		ND
BA18	362.2	MeOH	270	333	63	ND		ND

Maximum absorption wavelength (λ_{abs}^{max}), maximum emission wavelength (λ_{em}^{max}), Stokes shift (Δλ): calculated as the difference between λ_{abs}^{max} and λ_{em}^{max}, molar extinction coefficient (ε), fluorescence quantum yield (Φ_F): calculated by comparing to fluorescence reference standards with known quantum yield values such as Rhodamine B (Φ_F = 0.70 in EtOH), Quinine sulfate (Φ_F = 0.51 in 0.1 M H_2SO_4), and Brightness: this parameter was calculated using the formula: Brightness = Extinction Coefficient (ε) × Fluorescence Quantum Yield (Φ_F), ND = not determined.

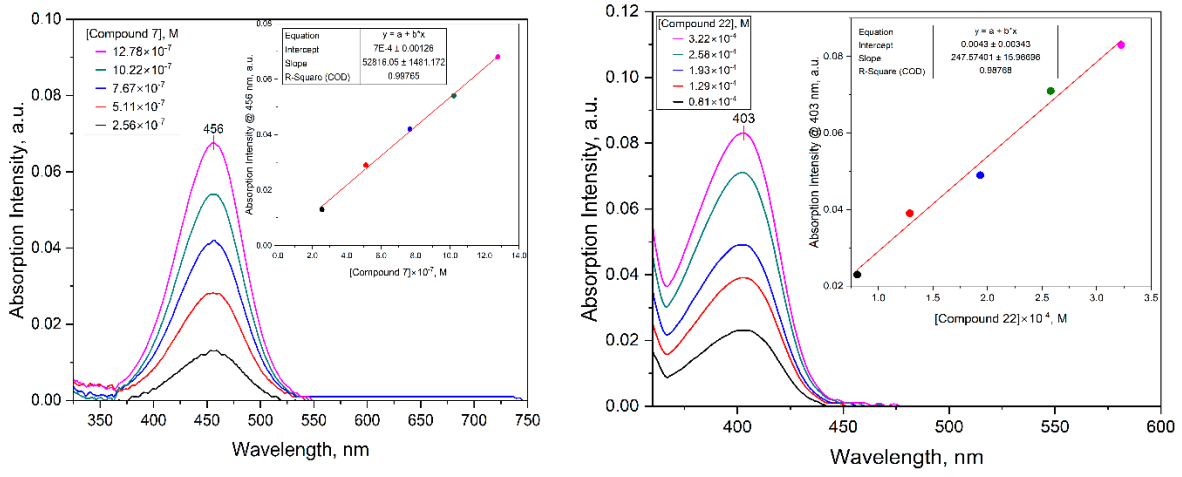

(**a**) (**b**)

Figure 9. Absorbance spectra of various dyes in different organic solvents; Insets: respective linearity plots for the evaluation of molar extinction coefficients (ε) for the dyes at the absorption maxima: (**a**) Compound **7**; (**b**) Compound **22.**

Additionally, the fluorescence emission curves were obtained by exciting the compounds at their respective absorption maxima. The normalized fluorescence emission spectra of the synthesized

 doi:10.20944/preprints202503.0093.v1

compounds are shown in Figures 10 and S90. The maximum emission bands are as follows; **37** (λ_{em} = 525 nm at λ_{ex} = 480 nm), **7** (λ_{em} = 590 nm at λ_{ex} = 456 nm), **29** (λ_{em} = 405 nm at λ_{ex} = 318 nm), **36** (λ_{em} = 347 nm at λ_{ex} = 301 nm), **22** (λ_{em} = 448 nm at λ_{ex} = 403 nm), **39** (λ_{em} = 569 nm at λ_{ex} = 540 nm), and **45** (λ_{em} = 508 nm at λ_{ex} = 496 nm). The Stokes shift ($\Delta\lambda$) – defined as the difference between absorption maxima (λ_{abs}^{max}) and emission maxima (λ_{em}^{max}) was calculated for the various compounds. Fluorescence spectra of the varying concentrations of unknown samples and references with the absorbance values and integrated intensities (area under curve) of both samples and corresponding reference are shown in Table 2. The relative fluorescence quantum yield (Φ_F) was determined relative to Rhodamine B in ethanol and Quinine sulfate in 0.1 M H_2SO_4 from fluorescence measurements. Quantum yield measurements require low absorbance (optical density), typically below 0.1 at the longest wavelength absorption maxima. Therefore, all solutions of all synthesized arylboronic dyes were prepared at low concentrations to limit the absorbance values to less than 0.1 in order to avoid any complications with dimer or aggregate formation [136], reduce or minimize possible non-linear effects arising from the inner filter (reabsorption effects) [65,136], eliminate concentration quenching effects, internal filter effects and errors arising from uneven distribution of the excited species in the detected volume [66], which altogether may otherwise skew the resulting quantum yield.

Table 2. Absorbance, and Integrated fluorescence intensities (Areas) for various samples and References.

	Integrated Fluorescence Intensity	
Absorbance @ 499 nm	**7**	**Rhodamine B**
0.020	2619195.0	2549829.2
0.016	2158588.5	2121340.3
0.012	1682211.2	1495319.2
0.009	1204913.3	1066673.4
0.004	591676.7	415287.3
Slope	128197000.0	115445000.0
Absorbance @ 358 nm	**22**	**Quinine sulfate**
0.072	2384944.0	9169983.2
0.058	2080661.1	7757302.9
0.051	1560798.8	6858240.1
0.038	1032764.1	5131493.2
0.028	510273.4	3945263.9
Slope	43905200.0	120830000.0
Absorbance @ 332 nm	**29**	**Quinine sulfate**
0.080	406256.1	10254500.0
0.066	331390.9	8717544.0
0.053	269142.8	7633669.7
0.040	195980.9	5868201.1
0.030	134100.4	4435606.5
Slope	5383876.6	114494000.0
Absorbance @ 502.5 nm	**37**	**Rhodamine B**
0.023	2014294.3	2863728.4
0.020	1785124.7	2380927.6
0.014	1300128.5	1745938.7
0.010	942578.1	1216051.1
0.005	455519.6	489246.6
Slope	861649000.0	128111000.0
Absorbance @ 544.5 nm	**39**	**Rhodamine B**
0.078	6696547.2	8871962.3
0.064	6251111.1	7476185.8
0.048	4931408.8	5593976.4
0.032	3405442.5	3872951.0

 doi:10.20944/preprints202503.0093.v1

0.017	1858555.0	1555633.8
Slope	81524200.0	118451000.0
Absorbance @ 502.5 nm	**45**	**Rhodamine B**
0.023	3049627.7	2863728.4
0.019	2613267.2	2380927.6
0.014	1973366.8	1745938.7
0.010	1360672.8	1216051.1
0.005	731821.0	489246.6
Slope	127606000.0	128111000.0

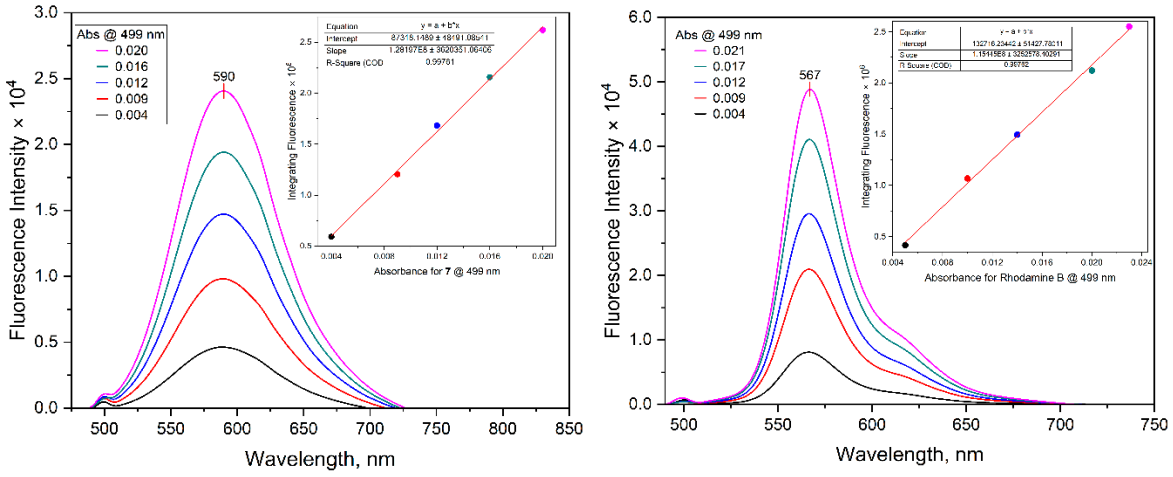

(**a**) (**b**)

Figure 10. Fluorescence emission spectra of synthesized compounds (left) and reference compounds (Rhodamine B or Quinine sulfate (right)) with varying absorbance. Inset: Calibration curves of integrated fluorescence intensity (area under curve) against absorbance for sample respectively: (a) Compound **7**; (b) Rhodamine B at 499 nm.

Finally, the brightness of each of the synthesized dyes was calculated from the molar absorption coefficient at the excitation wavelength and the fluorescence quantum yield values. Brightness is defined as the product of ε and Φ_F ($B = \Phi_F \times \varepsilon$). The brightness values allow for more practically meaningful comparisons between different dyes and as a result, can be used to determine the analytical sensitivity from the fluorophore side [53,137,138]. From the data obtained, the fluorescence emissions of most of the compounds occurred at longer wavelengths in the visible region of the electromagnetic spectrum as compared to the absorption spectra. This can be explained by the general principle that there are usually energy losses associated with absorption and emission spectra, thus, shifting the fluorescence spectra to longer wavelengths [139]. The fluorescence observed can be attributed to n→π* or π→π* transition states [140]. The Δλ values ranged from the least for **45** (Δλ = 12 nm) to sufficiently large Stokes shift values (Δλ > 80 nm) for **29**, **7**, and **24** with Δλ values of 87, 134, and 180.5 nm respectively. The BODIPY analogue **45** showed an intense absorption band with a maximum at 496 nm assigned at spin-allowed π-π* transitions, high molar extinction coefficient (ε = 29259 ± 450 $M^{-1}cm^{-1}$ at 496 nm), emission maximum at 508 nm with the lowest calculated Δλ value of 12 nm. These properties are characteristic of the BODIPY chromophore subunits and consistent with reported data [119,141]. On the other hand, **7** with a high Δλ value of 134 nm has the coumarin core moiety.

Some of the synthesized compounds such as **47a–47c** did not show fluorescence. Incidentally, all three compounds are azo dyes and this was not surprising because as a general rule, these categories of dyes do not fluoresce [142]. Here, the absorbed energy is dissipated by the medium or emitted as phosphorescence, which has a longer lifetime for the excited state [140]. However, all three synthesized azo dyes were characterized by high molar extinction coefficient values for example **47a**

 doi:10.20944/preprints202503.0093.v1

(ε = 21696 ± 1997 $M^{-1}cm^{-1}$ at 464 nm), **47b** (ε = 20551 ± 360 $M^{-1}cm^{-1}$ at 416 nm), and **47c** (ε = 27245 ± 467 $M^{-1}cm^{-1}$ at 398 nm). The quantum yields for these dyes were not determined due to a lack of significant fluorescence emissions at their respective absorption maxima values and also because very small quantum yield values have been acquired for other azo dyes [143,144]. Unlike the azo dyes **47a–47c**, this was not the case for **48**, a Sudan I boronic acid derivative which is also an azo dye. Fluorescence was observed with **48** giving an emission maximum at 384 nm and a Δλ value of 49 nm. As a general principle, small-molecule fluorophores require a high degree of aromaticity to have absorptions in the visible region of the spectrum [4,139]. The compound with the largest molar extinction coefficient (ε = 52816 ± 1481 $M^{-1}cm^{-1}$ at 456 nm), Δλ value of 134 nm, Φ_F = 0.78 and brightness value (41196.6 $M^{-1}cm^{-1}$) was **7**, a coumarin derivative. This is typical of coumarin derivatives which are usually characterized by high molar extinction coefficients in the near-UV and visible range, high fluorescence emission and as a result, have found many uses as fluorescent chromophores for several applications [145,146].

Based on the excellent photophysical properties of **7**, its fluorescent properties toward mycolactone were investigated. Sensitive detection of mycolactone was achieved through fluorescence spectroscopy as shown in Figure 11. For instance, free **7** (2.5×10^{-3} mg/mL) exhibited weaker fluorescence intensity at the emission maximum of 581 nm. However, the fluorescence intensity gradually increased as the concentration of mycolactone increased from 0 to 8.0×10^{-3} mg/mL (0–1.6 equiv.). The enhanced fluorescence of **7** was also visually observed on f-TLC plates when coupled with mycolactone and under a 365 nm UV lamp, as shown in Figure 12.

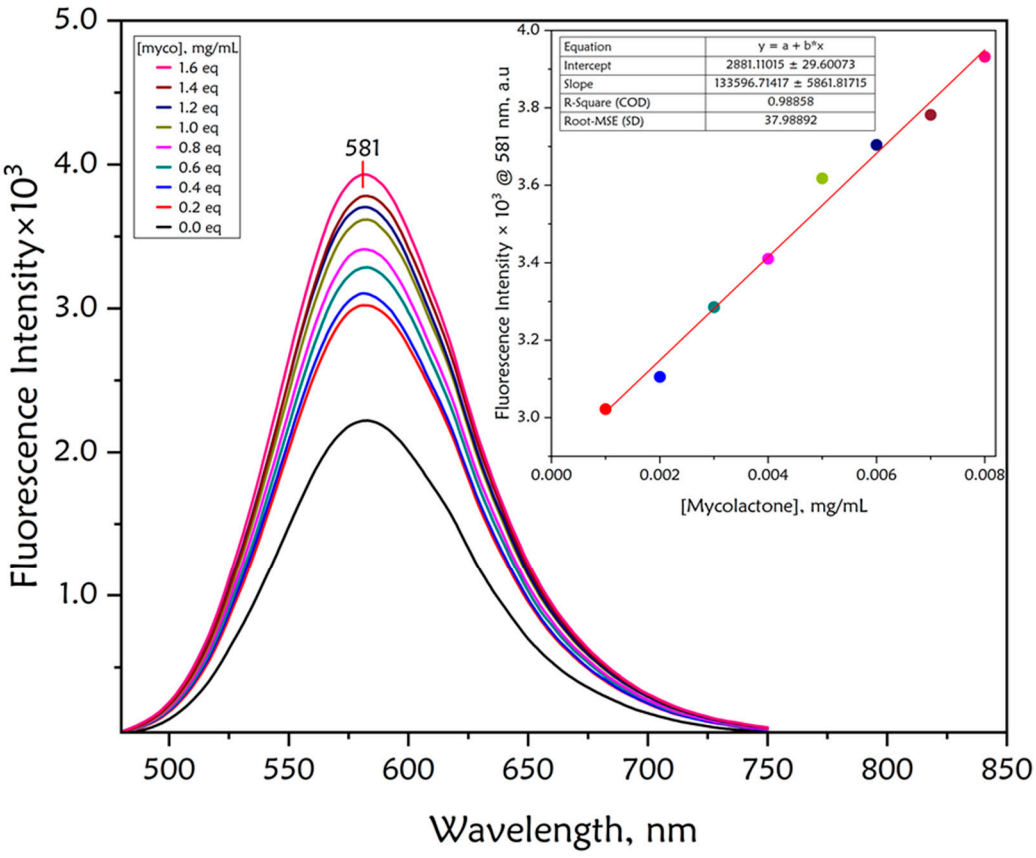

Figure 11. Fluorescence spectra of coumarin dye **7** (0.0025 mg/mL) upon gradual addition of serial concentrations of mycolactone (from bottom to top, 0 – 0.008 mg/mL) in ethanol. Inset: Plot of the linear relationship between the fluorescence intensity and varying concentrations of mycolactone.

 doi:10.20944/preprints202503.0093.v1

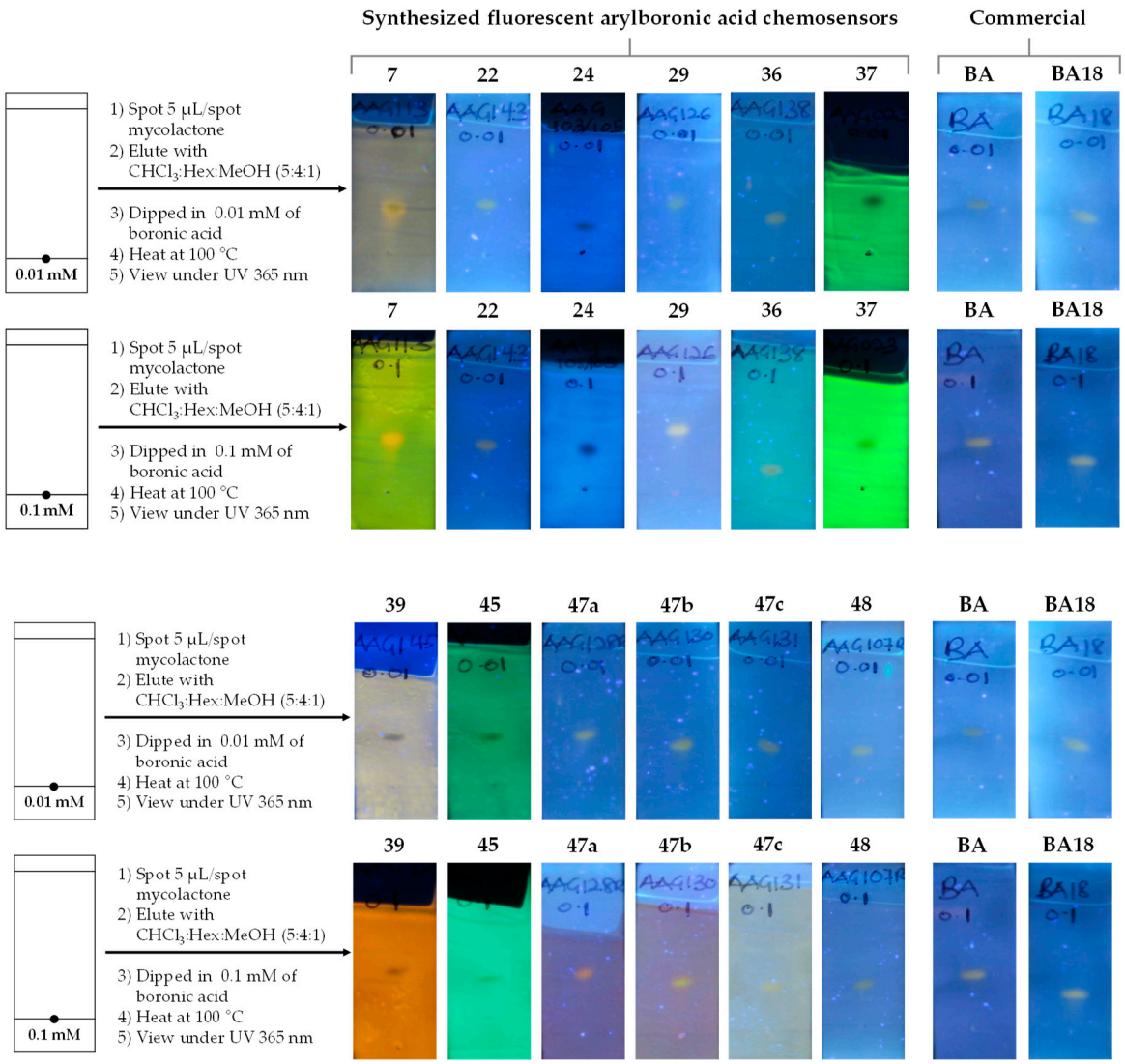

Figure 12. Images of the fluorescence response of 5 µL/spot of synthetic mycolactone after dipping in 0.1- and 0.01-mM acetone concentrations of various synthesized fluorescent aryl boronic acid chemosensors compared to two commercial boronic acids under 365 nm UV light.

This can be explained by the coupling of the boronic acid moiety in the structure of **7** with the 1,3-diol moieties of mycolactone to form 6-membered cyclic boronate esters as has been established in the previous section on the proof-of-concept studies. The formation of the boronate coupled with the chromophore of the mycolactone resulted in the enhanced fluorescence. A calibration curve was obtained between the concentration of mycolactone and fluorescence intensity at 581 nm with good linearity ($R^2 = 0.9886$) (**Inset,** Figure 11). The limit of detection (LOD) and limit of quantification (LOQ) were estimated to be 0.85 ng/µL (signal-to-noise ratio (S/N) × 3) and 2.84 ng/µL (signal-to-noise ratio (S/N) × 10) respectively; where *N* is the standard deviation (SD) of the peak area (n = 8), taken as a measure of the noise, and *B* is the slope of the corresponding calibration curve. This reveals that the **7** could detect a nanomolar-level concentration of mycolactone.

3.3. Detection of Mycolactone by the f-TLC Method Using the Synthesized Dyes

Boronic acids form reversible cyclic boronate complexes with 1,2- or 1,3-diols and this property. Neutral boronic acids are electrophilic because of the vacant *p*-orbital on the boron, and thus, are highly reactive toward nucleophiles, such as diols [147]. The interaction between a boronic acid and a diol is one of the most powerful functional group interactions [148]. This unique property makes boronic acids useful selective and sensitive detection reagents for diols in TLC. For instance, boronic

 doi:10.20944/preprints202503.0093.v1

acids have been employed in the detection of mycolactone on thin-layer chromatography (TLC) [45,46]. Here, the synthesized aryl boronic acids coupled to mycolactone and the resulting fluorescent boronate complexes were visualized under a benchtop UV lamp (365 nm). The detection of mycolactone spots on TLC plates was optimized by using different concentrations of the synthesized boronic acids. Figure 12 shows the images of the fluorescence response of 5 μL/spot of synthetic mycolactone after dipping in 0.1 mM and 0.01 mM acetone concentrations of various synthesized fluorescent aryl boronic acid chemosensors together with the two boronic acids previously reported for use in the f-TLC method which were obtained commercially (BA and BA18) [45,46,49].

First, a remarkable enhancement of fluorescence intensity of mycolactone was generally observed after dipping in either 0.01 mM or 0.1 mM solutions of the various boronic acids, particularly after heating. In this study, glass-backed TLC plates are used for the purpose of heating. Heating the plates to approximately 100 °C for just 60 seconds was sufficient to ensure the complete formation of the cyclic boronate esters of the various boronic acid sensors with the 1,3-diols motifs of the mycolactone. The boronic acid motif that is incorporated into various dyes has an empty sp^2 hybridized *p*-orbital on the boron centre with O–B–O bond angle of ~120°. It therefore readily binds covalently to 1,3-diols moieties of mycolactone and adopts sp^3 hybridization in the cyclic boronate ester product with the boron adopting a tetrahedral configuration with O–B–O ~109.5° as those in literature [147]. This then triggers a change in the spectroscopic properties of the adduct because of significant perturbation of the π system. Secondly, the enhanced fluorescence after coupling was also attributed to the various signalling moieties – aminoacridine, aminoquinoline, azo, BODIPY, coumarin, fluorescein, and rhodamine variants. They act as excellent fluorescent enhancers by stimulating the polarization of the C–B bond due to extended π-conjugation systems. This induced the production of a rapid signal because of the highly polar C–B bond along with the corresponding boronate unit.

Generally, it was observed that the fluorescence band intensities of mycolactone adducts on TLC plates dipped in 0.1 mM acetone solutions of the synthesized chemosensors appeared more intense than those dipped in the same concentration of the commercially available BA and BA18 solutions except for **37**, **48**, **47c**, **39**, and **45**. This observation was similar when 0.01 mM solutions of the boronic acids were used. Unlike other spots, it was observed that the mycolactone adduct spots appeared black on different backgrounds in solutions of **37**, **24, 39**, and **45**. Compound **37** produced the most intense black spot in the 0.01 mM solution while the **24** plate had the most intense black spot in the 0.1 mM solution.

Compounds **7**, **29**, **47a** and **47b** had outstanding fluorescent bands on TLC, especially in 0.1 mM solutions. In the case of **37**, **47c**, **36**, **39**, and **45** the mycolactone adduct of TLC plates dipped in 0.1 mM solutions showed weak fluorescent band intensities in comparison to the band intensities of plates that were dipped in the 10-fold lower concentrations of the same boronic acids. This could partly be a result of fluorescence quenching leading to the reduced fluorescence bands on TLC [140]. Should this be the case, then, this concentration range might be unsuitable for evaluating these boronic acids because of the dramatic concentration quenching of fluorescence.

 doi:10.20944/preprints202503.0093.v1

4. Conclusions

This paper has demonstrated synthetic approaches for the synthesis of a library of fluorescent arylboronic acid chemosensors by exploiting a range dyes (fluorophores) of interest with beneficial photophysical characteristics. All the synthesized molecules have a boronic acid motif (recognition moiety) linked to a fluorescent dye which serves as a signalling moiety for possible selective complexation with the 1,3-diol moieties of mycolactone. All the synthesized dyes have been completely characterized using a set of complementary spectrometric and spectroscopic techniques such as NMR, LC-MS, FT-IR, and in some cases, X-ray crystallography. Following the successful characterization of the synthesized dyes, their photophysical properties were determined. Likewise, their performance on TLC was also investigated in comparison to **BA** and **BA18**. The findings of the study indicated that the synthesized boronic acids were able to detect mycolactone both in solution and on TLC plates selectively and sensitively. From the results, it can be concluded that all the synthesized arylboronic acids are selective for the detection of mycolactone and **7** gave the best outcomes in terms of fluorescence on TLC plates. It returned λ_{abs}^{max} = 456 nm, λ_{em}^{max} = 590 nm, $\Delta\lambda$ = 134 nm, ε = 52816 $M^{-1}cm^{-1}$, Φ_F = 0.78, and brightness = 41197 $M^{-1}cm^{-1}$.

Supplementary Materials: The following supporting information can be downloaded at: Preprints.org.

Author Contributions: Conceptualization, G.A.A., B.M.P., T.D.C., and R.K.A.; methodology, G.A.A. B.M.P., T.D.C., and R.K.A.; validation, G.A.A., B.M.P., T.D.C., K.B.A. and R.K.A.; formal analysis, G.A.A., B.M.P., and R.K.A.; investigation, G.A.A. B.M.P., T.D.C., and R.K.A.; resources, B.M.P., K.B.A. and R.K.A.; data curation, G.A.A. B.M.P., and R.K.A.; writing—original draft preparation, G.A.A.; writing—review and editing, G.A.A., B.M.P., T.D.C., and R.K.A.; visualization, G.A.A.; supervision, B.M.P., T.D.C., and R.K.A.; project administration, R.K.A All authors have read and agreed to the published version of the manuscript.

Funding: "This research was not funded by any organization. Mass spectrometric, and X-ray crystallography analysis was performed at the University of Sheffield.

Institutional Review Board Statement: Not applicable.

Informed Consent Statement: Not applicable.

Data Availability Statement: Not applicable.

Acknowledgments: The authors are grateful to the late Professor Kishi Yoshito for generously donating synthetic mycolactone A/B through the World Health Organization for the study and to Erasmus+ mobility grant between University of Ghana and University of Sheffield and Ghana National Petroleum Company (GNPC) for funding Gideon Atinga Akolgo's Doctoral research.

Conflicts of Interest: The authors declare no conflicts of interest.

References

1. Whyte, G.F.; Vilar, R.; Woscholski, R. Molecular recognition with boronic acids—applications in chemical biology. *Journal of Chemical Biology* **2013**, *6*, 161-174.
2. Czarnik, A.W. *Chemosensors of ion and molecule recognition*; Springer Science & Business Media: 2012; Volume 492.
3. Wu, J.-S.; Liu, W.-M.; Zhuang, X.-Q.; Wang, F.; Wang, P.-F.; Tao, S.-L.; Zhang, X.-H.; Wu, S.-K.; Lee, S.-T. Fluorescence Turn on of Coumarin Derivatives by Metal Cations: A New Signaling Mechanism Based on C=N Isomerization. *Organic Letters* **2007**, *9*, 33-36.
4. Valeur, B.; Berberan-Santos, M.N. *Molecular fluorescence: principles and applications*; John Wiley & Sons: 2012.
5. Tharmaraj, V.; Pitchumani, K. d-Glucose sensing by (E)-(4-((pyren-1-ylmethylene)amino)phenyl) boronic acid via a photoinduced electron transfer (PET) mechanism. *RSC Advances* **2013**, *3*, 11566-11570.
6. Curtius, H.; Kaiser, G.; Müller, E.; Bosbach, D. Radionuclide release from research reactor spent fuel. *Journal of Nuclear Materials* **2011**, *416*, 211-215.

 doi:10.20944/preprints202503.0093.v1

7. Wu, X.; Chen, X.-X.; Jiang, Y.-B. Recent advances in boronic acid-based optical chemosensors. *Analyst* **2017**, *142*, 1403-1414.
8. Hall, D.G. Boronic Acids. **2011**.
9. Springsteen, G.; Wang, B. A detailed examination of boronic acid–diol complexation. *Tetrahedron* **2002**, *58*, 5291-5300.
10. Springsteen, G.; Wang, B. Alizarin Red S. as a general optical reporter for studying the binding of boronic acids with carbohydrates. *Chemical Communications* **2001**, 1608-1609.
11. Lorand, J.P.; EDWARDS, J.O. Polyol complexes and structure of the benzeneboronate ion. *The Journal of Organic Chemistry* **1959**, *24*, 769-774.
12. Yoon, J.; Czarnik, A.W. Fluorescent chemosensors of carbohydrates. A means of chemically communicating the binding of polyols in water based on chelation-enhanced quenching. *Journal of the American Chemical Society* **1992**, *114*, 5874-5875.
13. Guo, Z.; Shin, I.; Yoon, J. Recognition and sensing of various species using boronic acid derivatives. *Chemical Communications* **2012**, *48*, 5956-5967.
14. Lacina, K.; Skládal, P.; James, T.D. Boronic acids for sensing and other applications - a mini-review of papers published in 2013. *Chemistry Central Journal* **2014**, *8*, 60.
15. Chaicham, A.; Sahasithiwat, S.; Tuntulani, T.; Tomapatanaget, B. Highly effective discrimination of catecholamine derivatives via FRET-on/off processes induced by the intermolecular assembly with two fluorescence sensors. *Chemical Communications* **2013**, *49*, 9287-9289.
16. Kaur, G.; Fang, H.; Gao, X.; Li, H.; Wang, B. Substituent effect on anthracene-based bisboronic acid glucose sensors. *Tetrahedron* **2006**, *62*, 2583-2589.
17. Wu, W.; Mitra, N.; Yan, E.C.; Zhou, S. Multifunctional hybrid nanogel for integration of optical glucose sensing and self-regulated insulin release at physiological pH. *Acs Nano* **2010**, *4*, 4831-4839.
18. Wu, W.; Zhou, T.; Berliner, A.; Banerjee, P.; Zhou, S. Glucose-Mediated Assembly of Phenylboronic Acid Modified CdTe/ZnTe/ZnS Quantum Dots for Intracellular Glucose Probing. *Angewandte Chemie International Edition* **2010**, *49*, 6554-6558.
19. Huang, Y.-J.; Ouyang, W.-J.; Wu, X.; Li, Z.; Fossey, J.S.; James, T.D.; Jiang, Y.-B. Glucose sensing via aggregation and the use of "knock-out" binding to improve selectivity. *Journal of the American Chemical Society* **2013**, *135*, 1700-1703.
20. Zhai, W.; Male, L.; Fossey, J.S. Glucose selective bis-boronic acid click-fluor. *Chemical Communications* **2017**, *53*, 2218-2221.
21. Whyte, G.F.; Vilar, R.; Woscholski, R. Molecular recognition with boronic acids-applications in chemical biology. *J Chem Biol* **2013**, *6*, 161-174.
22. Pohanka, M. Glycated Hemoglobin and Methods for Its Point of Care Testing. *Biosensors* **2021**, *11*, 70.
23. Zhu, X.; Zhou, X.; Xing, D. Ultrasensitive and selective detection of mercury (II) in aqueous solution by polymerase assisted fluorescence amplification. *Biosensors and Bioelectronics* **2011**, *26*, 2666-2669.
24. Guan, R.; Chen, H.; Cao, F.; Cao, D.; Deng, Y. Two fluorescence turn-on chemosensors for cyanide anions based on pyridine cation and the boronic acid moiety. *Inorganic Chemistry Communications* **2013**, *38*, 112-114.
25. Lee, S.A.; You, G.R.; Choi, Y.W.; Jo, H.Y.; Kim, A.R.; Noh, I.; Kim, S.-J.; Kim, Y.; Kim, C. A new multifunctional Schiff base as a fluorescence sensor for Al 3+ and a colorimetric sensor for CN− in aqueous media: an application to bioimaging. *Dalton Transactions* **2014**, *43*, 6650-6659.
26. Pizer, R.; Tihal, C. Equilibria and reaction mechanism of the complexation of methylboronic acid with polyols. *Inorganic chemistry* **1992**, *31*, 3243-3247.
27. Pizer, R.D.; Tihal, C.A. Mechanism of boron acid/polyol complex formation. comments on the trigonal/tetrahedral interconversion on boron. *Polyhedron* **1996**, *15*, 3411-3416.
28. DeFrancesco, H.; Dudley, J.; Coca, A. Boron chemistry: an overview. *Boron reagents in synthesis* **2016**, 1-25.
29. Ooyama, Y.; Furue, K.; Uenaka, K.; Ohshita, J. Development of highly-sensitive fluorescence PET (photo-induced electron transfer) sensor for water: Anthracene–boronic acid ester. *RSC Advances* **2014**, *4*, 25330-25333.

 doi:10.20944/preprints202503.0093.v1

30. Ooyama, Y.; Matsugasako, A.; Oka, K.; Nagano, T.; Sumomogi, M.; Komaguchi, K.; Imae, I.; Harima, Y. Fluorescence PET (photo-induced electron transfer) sensors for water based on anthracene–boronic acid ester. *Chemical Communications* **2011**, *47*, 4448-4450.
31. Chung, C.; Srikun, D.; Lim, C.S.; Chang, C.J.; Cho, B.R. A two-photon fluorescent probe for ratiometric imaging of hydrogen peroxide in live tissue. *Chemical Communications* **2011**, *47*, 9618-9620.
32. Nonaka, H.; An, Q.; Sugihara, F.; Doura, T.; Tsuchiya, A.; Yoshioka, Y.; Sando, S. Phenylboronic Acid-based 19F MRI Probe for the Detection and Imaging of Hydrogen Peroxide Utilizing Its Large Chemical-Shift Change. *analytical sciences* **2015**, *31*, 331-335.
33. Fu, H.; Fang, H.; Sun, J.; Wang, H.; Liu, A.; Sun, J.; Wu, Z. Boronic acid-based enzyme inhibitors: a review of recent progress. *Current Medicinal Chemistry* **2014**, *21*, 3271-3280.
34. Cai, B.; Luo, Y.; Guo, Q.; Zhang, X.; Wu, Z. A glucose-sensitive block glycopolymer hydrogel based on dynamic boronic ester bonds for insulin delivery. *Carbohydrate research* **2017**, *445*, 32-39.
35. Fang, H.; Kaur, G.; Wang, B. Progress in boronic acid-based fluorescent glucose sensors. *Journal of Fluorescence* **2004**, *14*, 481-489.
36. Chang, M.-H.; Chang, C.-N. Synthesis of three fluorescent boronic acid sensors for tumor marker Sialyl Lewis X in cancer diagnosis. *Tetrahedron Letters* **2014**, *55*, 4437-4441.
37. Chu, Y.; Wang, D.; Wang, K.; Liu, Z.L.; Weston, B.; Wang, B. Fluorescent conjugate of sLex-selective bisboronic acid for imaging application. *Bioorganic & medicinal chemistry letters* **2013**, *23*, 6307-6309.
38. George, K.M.; Chatterjee, D.; Gunawardana, G.; Welty, D.; Hayman, J.; Lee, R.; Small, P.L. Mycolactone: a polyketide toxin from Mycobacterium ulcerans required for virulence. *Science* **1999**, *283*, 854-857.
39. Demangel, C.; Stinear, T.P.; Cole, S.T. Buruli ulcer: reductive evolution enhances pathogenicity of Mycobacterium ulcerans. *Nat Rev Microbiol* **2009**, *7*.
40. George, K.M.; Pascopella, L.; Welty, D.M.; Small, P.L. A Mycobacterium ulcerans toxin, mycolactone, causes apoptosis in guinea pig ulcers and tissue culture cells. *Infect Immun* **2000**, *68*, 877-883.
41. Scherr, N.; Gersbach, P.; Dangy, J.P.; Bomio, C.; Li, J.; Altmann, K.H.; Pluschke, G. Structure-activity relationship studies on the macrolide exotoxin mycolactone of Mycobacterium ulcerans. *PLoS Negl Trop Dis* **2013**, *7*, e2143.
42. Saint-Auret, S.; Chany, A.C.; Casarotto, V.; Tresse, C.; Parmentier, L.; Abdelkafi, H.; Blanchard, N. Total Syntheses of Mycolactone A/B and its Analogues for the Exploration of the Biology of Buruli Ulcer. *Chimia (Aarau)* **2017**, *71*, 836-840.
43. Hong, H.; Coutanceau, E.; Leclerc, M.; Caleechurn, L.; Leadlay, P.F.; Demangel, C. Mycolactone diffuses from Mycobacterium ulcerans–infected tissues and targets mononuclear cells in peripheral blood and lymphoid organs. *PLoS neglected tropical diseases* **2008**, *2*, e325.
44. Sarfo, F.S.; Phillips, R.O.; Rangers, B.; Mahrous, E.A.; Lee, R.E.; Tarelli, E.; Asiedu, K.B.; Small, P.L.; Wansbrough-Jones, M.H. Detection of Mycolactone A/B in Mycobacterium ulcerans-Infected Human Tissue. *PLoS Negl Trop Dis* **2010**, *4*, e577.
45. Akolgo, G.A.; Partridge, B.M.; D. Craggs, T.; Amewu, R.K. Alternative boronic acids in the detection of Mycolactone A/B using the thin layer chromatography (f-TLC) method for diagnosis of Buruli ulcer. *BMC Infectious Diseases* **2023**, *23*, 495.
46. Spangenberg, T.; Kishi, Y. Highly sensitive, operationally simple, cost/time effective detection of the mycolactones from the human pathogen Mycobacterium ulcerans. *Chemical communications* **2010**, *46*, 1410-1412.
47. Kishi, Y. Chemistry of mycolactones, the causative toxins of Buruli ulcer. *Proc Natl Acad Sci U S A* **2011**, *108*, 6703-6708.
48. Converse, P.J.; Xing, Y.; Kim, K.H.; Tyagi, S.; Li, S.Y.; Almeida, D.V.; Nuermberger, E.L.; Grosset, J.H.; Kishi, Y. Accelerated detection of mycolactone production and response to antibiotic treatment in a mouse model of Mycobacterium ulcerans disease. *PLoS Negl Trop Dis* **2014**, *8*, e2618.
49. Amewu, R.K.; Akolgo, G.A.; Asare, M.E.; Abdulai, Z.; Ablordey, A.S.; Asiedu, K. Evaluation of the fluorescent-thin layer chromatography (f-TLC) for the diagnosis of Buruli ulcer disease in Ghana. *PLOS ONE* **2022**, *17*, e0270235.

 doi:10.20944/preprints202503.0093.v1

50. Wadagni, A.; Frimpong, M.; Phanzu, D.M. Simple, rapid Mycobacterium ulcerans disease diagnosis from clinical samples by fluorescence of mycolactone on thin layer chromatography. *PLoS Negl Trop Dis* **2015**, *9*.
51. Yuan, L.; Lin, W.; Yang, Y.; Chen, H. A unique class of near-infrared functional fluorescent dyes with carboxylic-acid-modulated fluorescence ON/OFF switching: rational design, synthesis, optical properties, theoretical calculations, and applications for fluorescence imaging in living animals. *Journal of the American Chemical Society* **2012**, *134*, 1200-1211.
52. Yang, X.-F.; Guo, X.-Q.; Zhao, Y.-B. Development of a novel rhodamine-type fluorescent probe to determine peroxynitrite. *Talanta* **2002**, *57*, 883-890.
53. Lavis, L.D.; Raines, R.T. Bright building blocks for chemical biology. *ACS chemical biology* **2014**, *9*, 855-866.
54. Sheldrick, G.M. Program for empirical absorption correction of area detector data. *SADABS* **1996**.
55. Krause, L.; Herbst-Irmer, R.; Sheldrick, G.M.; Stalke, D. Comparison of silver and molybdenum microfocus X-ray sources for single-crystal structure determination. *Journal of applied crystallography* **2015**, *48*, 3-10.
56. Blessing, R.H. An empirical correction for absorption anisotropy. *Acta Crystallographica Section A: Foundations of Crystallography* **1995**, *51*, 33-38.
57. Sheldrick, G. SHELXT - Integrated space-group and crystal-structure determination. *Acta Crystallographica Section A* **2015**, *71*, 3-8.
58. Sheldrick, G. Crystal structure refinement with SHELXL. *Acta Crystallographica Section C* **2015**, *71*, 3-8.
59. Dolomanov, O.; Bourhis, L.; Gildea, R.; Howard, J.; Puschmann, H. _journal_name_full'American Mineralogist'_journal_year 2021 _journal_volume 106 _journal_page_first 1844 _journal_paper_doi 10.2138/am-2021-7785. *J. Appl. Cryst* **2009**, *42*, 339-341.
60. Ishiyama, T.; Murata, M.; Miyaura, N. Palladium(0)-Catalyzed Cross-Coupling Reaction of Alkoxydiboron with Haloarenes: A Direct Procedure for Arylboronic Esters. *The Journal of Organic Chemistry* **1995**, *60*, 7508-7510.
61. Akgun, B. Boronic Esters as Bioorthogonal Probes in Site-Selective Labeling of Proteins. **2018**.
62. Ear, A.; Amand, S.; Blanchard, F.; Blond, A.; Dubost, L.; Buisson, D.; Nay, B. Direct biosynthetic cyclization of a distorted paracyclophane highlighted by double isotopic labelling of l-tyrosine. *Organic & Biomolecular Chemistry* **2015**, *13*, 3662-3666.
63. Promchat, A.; Wongravee, K.; Sukwattanasinitt, M.; Praneenararat, T. Rapid Discovery and Structure-Property Relationships of Metal-Ion Fluorescent Sensors via Macroarray Synthesis. *Scientific Reports* **2019**, *9*, 10390.
64. Lawson-Wood, K.; Upstone, S.; Evans, K. Determination of Relative Fluorescence Quantum Yields using the FL6500 Fluorescence Spectrometer. *Fluoresc. Spectrosc* **2018**, *4*, 1-5.
65. Würth, C.; Grabolle, M.; Pauli, J.; Spieles, M.; Resch-Genger, U. Relative and absolute determination of fluorescence quantum yields of transparent samples. *Nature protocols* **2013**, *8*, 1535-1550.
66. Brouwer, A.M. Standards for photoluminescence quantum yield measurements in solution (IUPAC Technical Report). *Pure and Applied Chemistry* **2011**, *83*, 2213-2228.
67. Velapoldi, R.A.; Mielenz, K. *A Fluorescence Standard Reference Material, Quinine Sulfate Dihydrate*; US Department of Commerce, National Bureau of Standards: 1980.
68. Herráez, J.V.; Belda, R. Refractive Indices, Densities and Excess Molar Volumes of Monoalcohols + Water. *Journal of Solution Chemistry* **2006**, *35*, 1315-1328.
69. Ishiyama, T.; Murata, M.; Miyaura, N. Palladium (0)-catalyzed cross-coupling reaction of alkoxydiboron with haloarenes: a direct procedure for arylboronic esters. *The Journal of Organic Chemistry* **1995**, *60*, 7508-7510.
70. Ishiyama, T.; Itoh, Y.; Kitano, T.; Miyaura, N. Synthesis of arylboronates via the palladium (0)-catalyzed cross-coupling reaction of tetra (alkoxo) diborons with aryl triflates. *Tetrahedron letters* **1997**, *38*, 3447-3450.
71. Ishiyama, T.; Ishida, K.; Miyaura, N. Synthesis of pinacol arylboronates via cross-coupling reaction of bis (pinacolato) diboron with chloroarenes catalyzed by palladium (0)–tricyclohexylphosphine complexes. *Tetrahedron* **2001**, *57*, 9813-9816.
72. Wu, C.; Wang, J.; Shen, J.; Bi, C.; Zhou, H. Coumarin-based Hg2+ fluorescent probe: Synthesis and turn-on fluorescence detection in neat aqueous solution. *Sensors and Actuators B: Chemical* **2017**, *243*, 678-683.

 doi:10.20944/preprints202503.0093.v1

73. Pang, B.-j.; Li, Q.; Li, C.-r.; Yang, Z.-y. A highly selective and sensitive coumarin derived fluorescent probe for detecting Hg2+ in 100% aqueous solutions. *Journal of Luminescence* **2019**, *205*, 446-450.
74. Ma, S.; Wang, K.-N.; Xing, M.; Feng, F.; Pan, Q.; Cao, D. A coumarin-boronic ester derivative as fluorescent chemosensor for detecting H2O2 in living cells. *Inorganic Chemistry Communications* **2021**, *124*, 108414.
75. Lin, C.; Zhang, M.; Yan, X.; Zhang, R.; He, X.; Yuan, Y. A Coumarin-boronic Based Fluorescent "ON-OFF" Probe for Hg2+ in Aqueous Solution. *Zeitschrift für anorganische und allgemeine Chemie* **2020**, *646*, 1892-1899.
76. Li, Q.; Hu, Y.; Hou, H.-N.; Yang, W.-N.; Hu, S.-L. A new coumarin-carbonothioate-based turn-on fluorescent chemodosimeter for selective detection of Hg2+. *Inorganica Chimica Acta* **2018**, *471*, 705-708.
77. Abdallah, M.; Hijazi, A.; Graff, B.; Fouassier, J.-P.; Rodeghiero, G.; Gualandi, A.; Dumur, F.; Cozzi, P.G.; Lalevée, J. Coumarin derivatives as versatile photoinitiators for 3D printing, polymerization in water and photocomposite synthesis. *Polymer Chemistry* **2019**, *10*, 872-884.
78. Wang, Y.; Li, Y.; Yu, T.; Su, W.; Ma, H.; Zhao, Y.; Li, X.; Zhang, H. Functionalized coumarin derivatives containing aromatic-imidazole unit as organic luminescent materials. *Dyes and Pigments* **2020**, *173*, 107958.
79. Klinck, R.; Stothers, J. Nuclear Magnetic Resonance Studies: Part I. The Chemical Shift of the Formyl Proton in Aromatic Aldehydes. *Canadian Journal of Chemistry* **1962**, *40*, 1071-1081.
80. Bai, H.; Sun, Q.; Tian, H.; Qian, J.; Zhang, L.; Zhang, W. A Long-Wavelength Fluorescent Probe for Saccharides Based on Boronic-Acid Receptor. *Chinese Journal of Chemistry* **2013**, *31*, 1095-1101.
81. Akgun, B.; Hall, D.G. Fast and Tight Boronate Formation for Click Bioorthogonal Conjugation. *Angewandte Chemie* **2016**, *128*, 3977-3981.
82. Moriya, T. Excited-state reactions of coumarins. VII. The solvent-dependent fluorescence of 7-hydroxycoumarins. *Bulletin of the Chemical Society of Japan* **1988**, *61*, 1873-1886.
83. Aaron, J.-J.; Buna, M.; Parkanyi, C.; Antonious, M.S.; Tine, A.; Cisse, L. Quantitative treatment of the effect of solvent on the electronic absorption and fluorescence spectra of substituted coumarins: Evaluation of the first excited singlet-state dipole moments. *Journal of fluorescence* **1995**, *5*, 337-347.
84. Palanisamy, S.; Wu, P.-Y.; Wu, S.-C.; Chen, Y.-J.; Tzou, S.-C.; Wang, C.-H.; Chen, C.-Y.; Wang, Y.-M. In vitro and in vivo imaging of peroxynitrite by a ratiometric boronate-based fluorescent probe. *Biosensors and Bioelectronics* **2017**, *91*, 849-856.
85. Wang, C.; Wang, P.; Liu, X.; Fu, J.; Xue, K.; Xu, K. Novel enantioselective fluorescent sensors for tartrate anion based on acridinezswsxa. *Luminescence* **2017**, *32*, 1313-1318.
86. Dai, Y.; Xu, K.; Li, Q.; Wang, C.; Liu, X.; Wang, P. Acridine-based complex as amino acid anion fluorescent sensor in aqueous solution. *Spectrochimica Acta Part A: Molecular and Biomolecular Spectroscopy* **2016**, *157*, 1-5.
87. Wang, C.; Fu, J.; Yao, K.; Xue, K.; Xu, K.; Pang, X. Acridine-based fluorescence chemosensors for selective sensing of Fe3+ and Ni2+ ions. *Spectrochimica Acta Part A: Molecular and Biomolecular Spectroscopy* **2018**, *199*, 403-411.
88. Turan-Zitouni, G.; Kaplancikli, Z.; Uçucu, Ü.; Özdemir, A.; Chevallet, P.; Tunali, Y. Synthesis of some 2-[(benzazole-2-yl) thio]-diphenylmethylacetamide derivatives and their antimicrobial activity. *Phosphorus, Sulfur, and Silicon* **2004**, *179*, 2183-2188.
89. Kaplancikli, Z.A.; Turan-Zitouni, G.; Revial, G.; Guven, K. Synthesis and study of antibacterial and antifungal activities of novel 2-[[(benzoxazole/benzimidazole-2-yl) sulfanyl] acetylamino] thiazoles. *Archives of pharmacal research* **2004**, *27*, 1081-1085.
90. Demir Özkay, Ü.; Özkay, Y.; Can, Ö.D. Synthesis and analgesic effects of 2-(2-carboxyphenylsulfanyl)-N-(4-substitutedphenyl) acetamide derivatives. *Medicinal Chemistry Research* **2011**, *20*, 152-157.
91. Olszewska, A.; Pohl, R.; Brázdová, M.; Fojta, M.; Hocek, M. Chloroacetamide-Linked Nucleotides and DNA for Cross-Linking with Peptides and Proteins. *Bioconjugate Chemistry* **2016**, *27*, 2089-2094.
92. Czaplinska, B.; Spaczynska, E.; Musiol, R. Quinoline fluorescent probes for zinc–from diagnostic to therapeutic molecules in treating neurodegenerative diseases. *Medicinal Chemistry* **2018**, *14*, 19-33.
93. Sousa, K.A.P.; Lima, F.M.R.; Monteiro, T.O.; Silva, S.M.; Goulart, M.O.F.; Damos, F.S.; Luz, R.d.C.S. Amperometric Photosensor Based on Acridine Orange/TiO 2 for Chlorogenic Acid Determination in Food Samples. *Food Analytical Methods* **2018**, *11*, 2731-2741.

 doi:10.20944/preprints202503.0093.v1

94. López-Soria, J.M.; Pérez, S.J.; Hernández, J.N.; Ramírez, M.A.; Martín, V.S.; Padrón, J.I. A practical, catalytic and selective deprotection of a Boc group in N,N′-diprotected amines using iron(iii)-catalysis. *RSC Advances* **2015**, *5*, 6647-6651.
95. Han, G.; Tamaki, M.; Hruby, V. Fast, efficient and selective deprotection of the tert-butoxycarbonyl (Boc) group using HCl/dioxane (4 m). *The Journal of Peptide Research* **2001**, *58*, 338-341.
96. Han, G.; Tamaki, M.; Hruby, V. Fast, efficient and selective deprotection of the tert-butoxycarbonyl (Boc) group using HCL/dioxane (4 M). *The journal of peptide research : official journal of the American Peptide Society* **2001**, *58*, 338-341.
97. Abdel-Magid, A.F.; Carson, K.G.; Harris, B.D.; Maryanoff, C.A.; Shah, R.D. Reductive amination of aldehydes and ketones with sodium triacetoxyborohydride. studies on direct and indirect reductive amination procedures1. *The Journal of organic chemistry* **1996**, *61*, 3849-3862.
98. Rahman, A.F.M.M.; Park, S.-E.; Kadi, A.A.; Kwon, Y. Fluorescein Hydrazones as Novel Nonintercalative Topoisomerase Catalytic Inhibitors with Low DNA Toxicity. *Journal of Medicinal Chemistry* **2014**, *57*, 9139-9151.
99. Kaschula, C.H.; Hunter, R. Synthesis and structure–activity relations in allylsulfide and isothiocyanate compounds from garlic and broccoli against in vitro cancer cell growth. *Studies in Natural Products Chemistry* **2016**, *50*, 1-43.
100. Podhradský, D.; Drobnica, Ľ.; Kristian, P. Reactions of cysteine, its derivatives, glutathione, coenzyme A, and dihydrolipoic acid with isothiocyanates. *Experientia* **1979**, *35*, 154-155.
101. Beija, M.; Afonso, C.A.; Martinho, J.M. Synthesis and applications of Rhodamine derivatives as fluorescent probes. *Chemical Society Reviews* **2009**, *38*, 2410-2433.
102. Kim, H.N.; Lee, M.H.; Kim, H.J.; Kim, J.S.; Yoon, J. A new trend in rhodamine-based chemosensors: application of spirolactam ring-opening to sensing ions. *Chemical Society Reviews* **2008**, *37*, 1465-1472.
103. Lee, V.Y.; Sekiguchi, A.; Kim, J.S.; Yoon, J. Biology terface. *Chem. Soc. Rev* **2008**, *37*, 1465-1472.
104. Wu, D.; Huang, W.; Duan, C.; Lin, Z.; Meng, Q. Highly sensitive fluorescent probe for selective detection of Hg2+ in DMF aqueous media. *Inorganic Chemistry* **2007**, *46*, 1538-1540.
105. Yang, Y.-K.; Yook, K.-J.; Tae, J. A Rhodamine-Based Fluorescent and Colorimetric Chemodosimeter for the Rapid Detection of Hg2+ Ions in Aqueous Media. *Journal of the American Chemical Society* **2005**, *127*, 16760-16761.
106. Kim, S.K.; Swamy, K.; Chung, S.-Y.; Kim, H.N.; Kim, M.J.; Jeong, Y.; Yoon, J. New fluorescent and colorimetric chemosensors based on the rhodamine and boronic acid groups for the detection of Hg2+. *Tetrahedron Letters* **2010**, *51*, 3286-3289.
107. Xiang, Y.; Tong, A.; Jin, P.; Ju, Y. New Fluorescent Rhodamine Hydrazone Chemosensor for Cu(II) with High Selectivity and Sensitivity. *Organic Letters* **2006**, *8*, 2863-2866.
108. Mao, J.; Wang, L.; Dou, W.; Tang, X.; Yan, Y.; Liu, W. Tuning the selectivity of two chemosensors to Fe (III) and Cr (III). *Organic letters* **2007**, *9*, 4567-4570.
109. Bossi, M.; Belov, V.; Polyakova, S.; Hell, S.W. Reversible red fluorescent molecular switches. *Angewandte Chemie International Edition* **2006**, *45*, 7462-7465.
110. Treibs, A.; Kreuzer, F.H. Difluorboryl-komplexe von di-und tripyrrylmethenen. *Justus Liebigs Annalen der Chemie* **1968**, *718*, 208-223.
111. Ojida, A.; Sakamoto, T.; Inoue, M.-a.; Fujishima, S.-h.; Lippens, G.; Hamachi, I. Fluorescent BODIPY-based Zn (II) complex as a molecular probe for selective detection of neurofibrillary tangles in the brains of Alzheimer's disease patients. *Journal of the American Chemical Society* **2009**, *131*, 6543-6548.
112. Smith, N.W.; Alonso, A.; Brown, C.M.; Dzyuba, S.V. Triazole-containing BODIPY dyes as novel fluorescent probes for soluble oligomers of amyloid Aβ1–42 peptide. *Biochemical and biophysical research communications* **2010**, *391*, 1455-1458.
113. Beatty, K.E.; Szychowski, J.; Fisk, J.D.; Tirrell, D.A. A BODIPY-cyclooctyne for protein imaging in live cells. *ChemBioChem* **2011**, *12*, 2137-2139.
114. Lin, H.-Y.; Huang, W.-C.; Chen, Y.-C.; Chou, H.-H.; Hsu, C.-Y.; Lin, J.T.; Lin, H.-W. BODIPY dyes with β-conjugation and their applications for high-efficiency inverted small molecule solar cells. *Chemical Communications* **2012**, *48*, 8913-8915.

 doi:10.20944/preprints202503.0093.v1

115. Altan Bozdemir, O.; Erbas-Cakmak, S.; Ekiz, O.O.; Dana, A.; Akkaya, E.U. Towards unimolecular luminescent solar concentrators: BODIPY-based dendritic energy-transfer cascade with panchromatic absorption and monochromatized emission. *Angewandte Chemie* **2011**, *123*, 11099-11104.
116. Rousseau, T.; Cravino, A.; Ripaud, E.; Leriche, P.; Rihn, S.; De Nicola, A.; Ziessel, R.; Roncali, J. A tailored hybrid BODIPY–oligothiophene donor for molecular bulk heterojunction solar cells with improved performances. *Chemical communications* **2010**, *46*, 5082-5084.
117. Karolin, J.; Johansson, L.B.-A.; Strandberg, L.; Ny, T. Fluorescence and absorption spectroscopic properties of dipyrrometheneboron difluoride (BODIPY) derivatives in liquids, lipid membranes, and proteins. *Journal of the American Chemical Society* **1994**, *116*, 7801-7806.
118. Kollmannsberger, M.; Gareis, T.; Heinl, S.; Daub, J.; Breu, J. Electrogenerated Chemiluminescence and Proton-Dependent Switching of Fluorescence: Functionalized Difluoroboradiaza-s-indacenes. *Angewandte Chemie International Edition in English* **1997**, *36*, 1333-1335.
119. Loudet, A.; Burgess, K. BODIPY dyes and their derivatives: syntheses and spectroscopic properties. *Chemical reviews* **2007**, *107*, 4891-4932.
120. Ulrich, G.; Ziessel, R.; Harriman, A. The chemistry of fluorescent bodipy dyes: versatility unsurpassed. *Angewandte Chemie International Edition* **2008**, *47*, 1184-1201.
121. Boens, N.; Leen, V.; Dehaen, W. Fluorescent indicators based on BODIPY. *Chemical Society Reviews* **2012**, *41*, 1130-1172.
122. Biagiotti, G.; Purić, E.; Urbančič, I.; Krišelj, A.; Weiss, M.; Mravljak, J.; Gellini, C.; Lay, L.; Chiodo, F.; Anderluh, M. Combining cross-coupling reaction and Knoevenagel condensation in the synthesis of glyco-BODIPY probes for DC-SIGN super-resolution bioimaging. *Bioorganic Chemistry* **2021**, *109*, 104730.
123. Mahato, P.; Saha, S.; Das, P.; Agarwalla, H.; Das, A. An overview of the recent developments on Hg 2+ recognition. *RSC Advances* **2014**, *4*, 36140-36174.
124. Bartelmess, J.; De Luca, E.; Signorelli, A.; Baldrighi, M.; Becce, M.; Brescia, R.; Nardone, V.; Parisini, E.; Echegoyen, L.; Pompa, P.P. Boron dipyrromethene (BODIPY) functionalized carbon nano-onions for high resolution cellular imaging. *Nanoscale* **2014**, *6*, 13761-13769.
125. Brückner, C.; Karunaratne, V.; Rettig, S.J.; Dolphin, D. Synthesis of meso-phenyl-4, 6-dipyrrins, preparation of their Cu (II), Ni (II), and Zn (II) chelates, and structural characterization of bis [meso-phenyl-4, 6-dipyrrinato] Ni (II). *Canadian journal of chemistry* **1996**, *74*, 2182-2193.
126. Shah, M.; Thangaraj, K.; Soong, M.L.; Wolford, L.T.; Boyer, J.H.; Politzer, I.R.; Pavlopoulos, T.G. Pyrromethene–BF2 complexes as laser dyes: 1. *Heteroatom Chemistry* **1990**, *1*, 389-399.
127. Jameson, L.P.; Dzyuba, S.V. Expeditious, mechanochemical synthesis of BODIPY dyes. *Beilstein Journal of Organic Chemistry* **2013**, *9*, 786-790.
128. Snyder, H.; Weaver, C. The preparation of some azo boronic acids. *Journal of the American Chemical Society* **1948**, *70*, 232-234.
129. Smoum, R.; Srebnik, M. Boronated saccharides: potential applications. *Studies in Inorganic Chemistry* **2005**, *22*, 391.
130. Egawa, Y.; Miki, R.; Seki, T. Colorimetric sugar sensing using boronic acid-substituted azobenzenes. *Materials* **2014**, *7*, 1201-1220.
131. Hansen, J.S.; Christensen, J.B.; Petersen, J.F.; Hoeg-Jensen, T.; Norrild, J.C. Arylboronic acids: A diabetic eye on glucose sensing. *Sensors and Actuators B: Chemical* **2012**, *161*, 45-79.
132. DiCesare, N.; Lakowicz, J.R. Spectral Properties of Fluorophores Combining the Boronic Acid Group with Electron Donor or Withdrawing Groups. Implication in the Development of Fluorescence Probes for Saccharides. *J Phys Chem A* **2001**, *105*, 6834-6840.
133. Beda, N.; Nedospasov, A. A spectrophotometric assay for nitrate in an excess of nitrite. *Nitric Oxide* **2005**, *13*, 93-97.
134. Sinan, R.; Al-Uzri, W.A. Spectrophotometric Method for Determination of Sulfamethoxazole in Pharmaceutical Preparations by Diazotization-Coupling Reaction. *Al-Nahrain Journal of Science* **2011**, *14*, 9-16.
135. Gordon, P.F.; Gregory, P. *Organic chemistry in colour*; Springer Science & Business Media: 2012.

 doi:10.20944/preprints202503.0093.v1

136. Dhami, S.; Mello, A.d.; Rumbles, G.; Bishop, S.; Phillips, D.; Beeby, A. Phthalocyanine fluorescence at high concentration: dimers or reabsorption effect? *Photochemistry and Photobiology* **1995**, *61*, 341-346.
137. Resch-Genger, U.; Grabolle, M.; Cavaliere-Jaricot, S.; Nitschke, R.; Nann, T. Quantum dots versus organic dyes as fluorescent labels. *Nature Methods* **2008**, *5*, 763-775.
138. Cavazos-Elizondo, D.; Aguirre-Soto, A. Photophysical Properties of Fluorescent Labels: A Meta-Analysis to Guide Probe Selection Amidst Challenges with Available Data. *Analysis & Sensing* **2022**, *2*, e202200004.
139. Lakowicz, J.R. *Principles of fluorescence spectroscopy*; Springer: 2006.
140. Spangenberg, B.; Poole, C.F.; Weins, C. *Quantitative thin-layer chromatography: a practical survey*; Springer Science & Business Media: 2011.
141. Giacomazzo, G.E.; Palladino, P.; Gellini, C.; Salerno, G.; Baldoneschi, V.; Feis, A.; Scarano, S.; Minunni, M.; Richichi, B. A straightforward synthesis of phenyl boronic acid (PBA) containing BODIPY dyes: new functional and modular fluorescent tools for the tethering of the glycan domain of antibodies. *RSC advances* **2019**, *9*, 30773-30777.
142. Isak, S.J.; Eyring, E.M.; Spikes, J.D.; Meekins, P.A. Direct blue dye solutions: photo properties. *Journal of Photochemistry and Photobiology A: Chemistry* **2000**, *134*, 77-85.
143. Dinçalp, H.; Toker, F.; Durucasu, İ.; Avcıbaşı, N.; Icli, S. New thiophene-based azo ligands containing azo methine group in the main chain for the determination of copper(II) ions. *Dyes and Pigments* **2007**, *75*, 11-24.
144. Joshi, H.; Kamounah, F.S.; Gooijer, C.; van der Zwan, G.; Antonov, L. Excited state intramolecular proton transfer in some tautomeric azo dyes and schiff bases containing an intramolecular hydrogen bond. *Journal of Photochemistry and Photobiology A: Chemistry* **2002**, *152*, 183-191.
145. Rahal, M.; Mokbel, H.; Graff, B.; Toufaily, J.; Hamieh, T.; Dumur, F.; Lalevée, J. Mono vs. difunctional coumarin as photoinitiators in photocomposite synthesis and 3D printing. *Catalysts* **2020**, *10*, 1202.
146. Rahal, M.; Graff, B.; Toufaily, J.; Hamieh, T.; Noirbent, G.; Gigmes, D.; Dumur, F.; Lalevée, J. 3-Carboxylic Acid and Formyl-Derived Coumarins as Photoinitiators in Photo-Oxidation or Photo-Reduction Processes for Photopolymerization upon Visible Light: Photocomposite Synthesis and 3D Printing Applications. *Molecules* **2021**, *26*, 1753.
147. Marco-Dufort, B.; Iten, R.; Tibbitt, M.W. Linking molecular behavior to macroscopic properties in ideal dynamic covalent networks. *Journal of the American Chemical Society* **2020**, *142*, 15371-15385.
148. Yan, J.; Fang, H.; Wang, B. Boronolectins and fluorescent boronolectins: An examination of the detailed chemistry issues important for the design. *Medicinal research reviews* **2005**, *25*, 490-520.